International Journal of Minerals, Metallurgy and Materials
Volume 28, Number 4, April 2021, Page 567
https://doi.org/10.1007/s12613-020-2216-8

Invited Review

Review on cyclic plasticity of magnesium alloys: Experiments and constitutive models

Guo-zheng Kang[1,2] *and Hang Li*[1]

1) Applied Mechanics and Structure Safety Key Laboratory of Sichuan Province, School of Mechanics and Engineering, Southwest Jiaotong University, Chengdu 610031, China

2) Institute of Applied Mechanics, State Key Laboratory of Traction Power, Southwest Jiaotong University, Chengdu 610031, China

(Received: 9 August 2020; revised: 26 October 2020; accepted: 27 October 2020)

Abstract: Fatigue analysis has always been a concern in the design and assessment of Mg alloy structure components subjected to cyclic loading, and research on the cyclic plasticity is fundamental to investigate the corresponding fatigue failure. Thus, this work reviews the progress in the cyclic plasticity of Mg alloys. First, the existing macroscopic and microscopic experimental results of Mg alloys are summarized. Then, corresponding macroscopic phenomenological constitutive models and crystal plasticity-based models are reviewed. Finally, some conclusions and recommended topics on the cyclic plasticity of Mg alloys are provided to boost the further development and application of Mg alloys.

Keywords: magnesium alloy; cyclic plasticity; macroscopic experiments; microscopic observations; constitutive model

1. Introduction

Magnesium (Mg) alloys have been widely applied in the aerospace, automobile, railway transportation, and biomedicine industries because of their light weight, high specific strength and stiffness, good damping capacity, and biocompatibility [1–4]. The fabricated components and devices inevitably undergo cyclic loading; then, the accumulation of the damage from the cyclic plasticity of Mg alloys in macro- or micro-scales may induce fatigue failure. To improve the capability of the assessment of the service reliability and fatigue life of structural components and devices, the cyclic plasticity of Mg alloys should be comprehensively studied.

Owing to their hexagonal close-packed structure, Mg alloys do not have sufficient active slip systems, and their plastic deformation is often accommodated by twinning. In general, the twinning can cause a rotation of crystal lattice at a large angle and remarkably change the orientation of slip systems in twinned regions. Additionally, the generation of twin boundaries has a significant impact on the dislocation slipping. Therefore, different plastic deformation mechanisms and complicated interactions among the twin boundaries will occur during the cyclic plasticity of Mg alloys. This implies that the cyclic plasticity of Mg alloys becomes more complicated due to the multi-mechanism interaction. A more comprehensive and deep investigation on the complex cyclic plasticity of Mg alloys has vital engineering and scientific significance.

In this work, the progresses in the macroscopic and microscopic experimental observations on the cyclic plasticity of Mg alloys and corresponding constitutive models are reviewed to promote the development and application of Mg alloys. First, the experiments conducted in current studies, including the macroscopic and microscopic observations, are summarized in Section 2, and the plastic deformation mechanisms and their interactions are addressed. Then, recently developed macroscopic phenomenological constitutive models and crystal plasticity-based models are reviewed in Section 3, and key ideas and the advantages and disadvantages of these constitutive models are discussed. Finally, significant conclusions and some recommendations are provided in Section 4.

2. Progresses in experimental observations

At present, many researchers have performed experimental observations on the cyclic plastic deformation of Mg alloys. The evolution features and physical mechanisms of cyclic plasticity have been investigated for Mg alloys, and valuable results have been obtained. The results are summar-

Corresponding author: Guo-zheng Kang E-mail: guozhengkang@home.swjtu.edu.cn, guozhengkang@126.com

ized in detail here in terms of macroscopic and microscopic observations.

2.1. Macroscopic experiments

Strain- and stress-controlled cyclic tests are two common cyclic loading modes used in experimental observations on the cyclic plasticity and related fatigue failure of materials, and through these tests, different cyclic deformation characteristics are observed. Thus, in this subsection, the macroscopic experimental observations on the cyclic plasticity of Mg alloys is summarized under two groups: strain- and stress-controlled loading modes. The corresponding physical mechanisms of cyclic plasticity revealed by the microscopic observations are reviewed in Section 2.2.

2.1.1. Strain-controlled cyclic plasticity

Wrought and cast Mg alloys are commonly used in engineering applications. However, a strong basal texture is formed during the extrusion and rolling of wrought Mg alloys; that is, the *c*-axis of most grains is almost perpendicular to the extrusion or rolling direction. Significant tension–compression asymmetry occurs in wrought Mg alloys because of their strong basal texture and different deformation mechanisms, including dislocation slipping, twinning, and detwinning, and their interaction [5–10]. Yield stresses and strain hardening features of wrought Mg alloys are different in the tensile and compressive directions, as shown in Fig. 1. The stress–strain curve of extruded AZ31B Mg alloy is typically convex-outward in the first tensile stage along the extrusion direction (ED), where the plastic deformation is dominated by dislocation slipping (Fig. 1(a)). In the second and first compressive stages with a lower yield stress, the plastic deformation is dominated by twinning (Figs. 1(a) and 1(b)), and then a sigmoidal-shaped (S-shaped) stress–strain curve appears in the reverse tensile stage due to the detwinning.

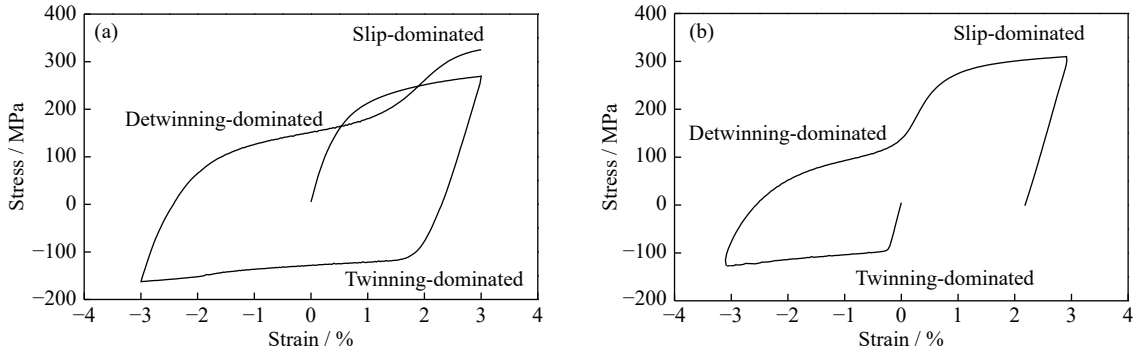

Fig. 1. Stress–strain responses of extruded AZ31B Mg alloy: (a) in a tension–compression–tension test; (b) in a compression–tension test. Reprinted from *Int. J. Fatigue*, 120, H. Li, G.Z. Kang, C. Yu, and Y.J. Liu, Experimental investigation on temperature-dependent uniaxial ratchetting of AZ31B magnesium alloy, 33-45, Copyright 2019, with permission from Elsevier.

For cast Mg alloys, since their grain orientations are randomly distributed without any strong textures, their plastic deformation is generally provided by dislocation slipping in the basal slip system and extension twinning [11]. In [11], the evolution trends of the tensile and compressive stress–strain curves of cast Mg alloys were almost the same; this observation is significantly different from the tension–compression asymmetry observed for the wrought Mg alloys, as shown in Fig. 1.

(1) Effects of strain amplitude.

Fully reversed uniaxial strain-controlled cyclic tests of wrought Mg alloys were performed in [12–19] under different strain amplitudes. Typical stress–strain curves of wrought Mg alloys with different strain amplitudes [18] are displayed in Fig. 2. As shown in the figure, normal convex-outward stress–strain curves occurred in the first tensile stage and the subsequent compressive stage with a smaller strain amplitude (i.e., 1%), but unique concave-inward stress–strain curves with inflection points occurred in the reverse tensile stages (Fig. 2(a)), which means that an S-shaped stress–strain curve occurred in the reverse tensile stage due to the detwinning; however, when the applied strain amplitude was 4%, S-shaped stress–strain curves occurred in both the compressive and reverse tensile stages (Fig. 2(b)); meanwhile, more significant cyclic hardening occurred in the compression stage than that in the tension stage. This was because the twins produced in the compressive stages were partially detwinned during subsequent reverse tensile stages, and the residual twins accumulated; the cyclic hardening in the compression also became more remarkable with the increase in the applied strain amplitude. Moreover, more symmetrical stress–strain responses occurred when the applied strain amplitude was large enough, since twinning was exhausted under the compression, and the subsequent plastic deformation in compression was dominated by dislocation slipping, which is similar to that in the reverse tension (i.e., detwinning followed by dislocation slipping). Xiong *et al.* [19] found similar strain amplitude–dependent cyclic plasticity in extruded AZ31 Mg alloy.

Since wrought Mg alloys possess strong basal textures,

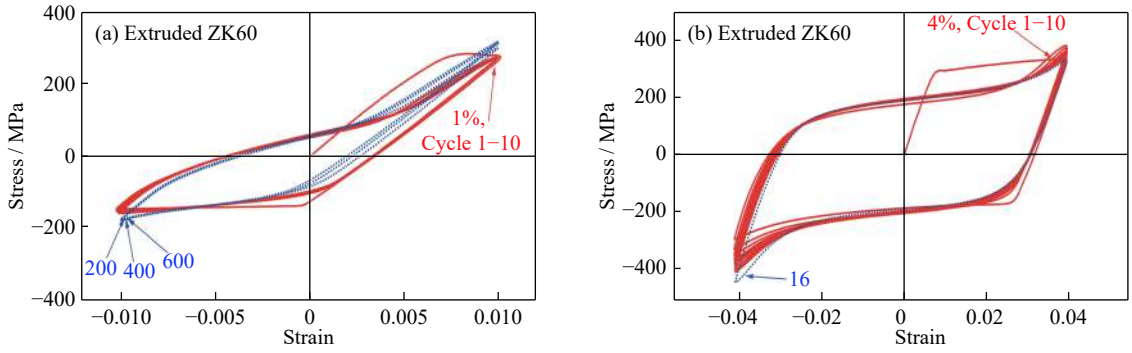

Fig. 2. Stress–strain curves in strain-controlled cyclic tests of extruded ZK60 Mg alloy with different strain amplitudes: (a) 1%; (b) 4%. Reprinted from *Int. J. Plast.*, 91, S. Dong, Q. Yu, Y.Y. Jiang, J. Dong, F.H. Wang, L. Jin, and W.J. Ding, Characteristic cyclic plastic deformation in ZK60 magnesium alloy, 25-47, Copyright 2017, with permission from Elsevier.

their strain amplitude–dependent cyclic plasticity also exhibits significant dependence on the loading direction. Pahlevanpour *et al.* [20] found that the stabilized stress–strain hysteresis loops of extruded ZK60 Mg alloy were asymmetrical in the ED when the strain amplitude was greater than 0.5%, due to the activation of twinning and detwinning, while those in the radial direction (RD) were roughly symmetrical under different strain amplitudes (from 0.2% to 2%). Wang *et al.* [21] obtained that both the stress–strain hysteresis loops of extruded ZA81M Mg alloy in the ED and the transverse direction (TD) were asymmetrical when the applied strain amplitude was between 0.4% and 1%, and significant cyclic hardening occurred in both directions. In summary, the strain amplitude has a remarkable impact on the cyclic plasticity of wrought Mg alloys, and the cyclic hardening extents and stress–strain hysteresis loop shapes during cyclic tests with different strain amplitudes are different, due to the different activated plastic deformation mechanisms.

For cast Mg alloys, Gryguc *et al.* [11] conducted some fully reversed cyclic tests of cast AZ80 Mg alloy under different strain amplitudes. The obtained stress–strain hysteresis loops were symmetrical and convex-outward (except for that under a strain amplitude of 1.4%, where a slight S-shaped looped occurred, as shown in Fig. 3), and significant cyclic hardening occurred; the mean stresses obtained in the cyclic tests of cast AZ80 Mg alloy under various strain amplitudes were almost zero, as shown in Fig. 3, different from that of wrought Mg alloys where a non-zero mean stress occurred even when the applied mean strain was zero (Fig. 2). Similar stress–strain hysteresis loops and cyclic hardening features have also been observed for cast ZK60 Mg alloy [22]; the study demonstrated that the larger the applied strain amplitude, the more remarkable the cyclic hardening. However, in [23], cyclic stability occurred in the fully reversed cyclic tests of cast high-zinc ZA105 Mg alloy under smaller strain amplitude (0.1% or 0.2%), but slight cyclic softening occurred when the applied strain amplitude was 0.6% or 0.8%. Moreover, tension–compression yield asymmetry has also been observed in some cast Mg alloys at the initial yielding stage, due to the different activations of extension twinning in tension and compression [24–25]. In these studies, the strain hardening features in tension and compression after the yielding were similar owing to the joint action of dislocation slipping and twinning, and symmetric stress–strain hysteresis loops occurred in the cyclic tests under a large applied strain amplitude. In summary, the influ-

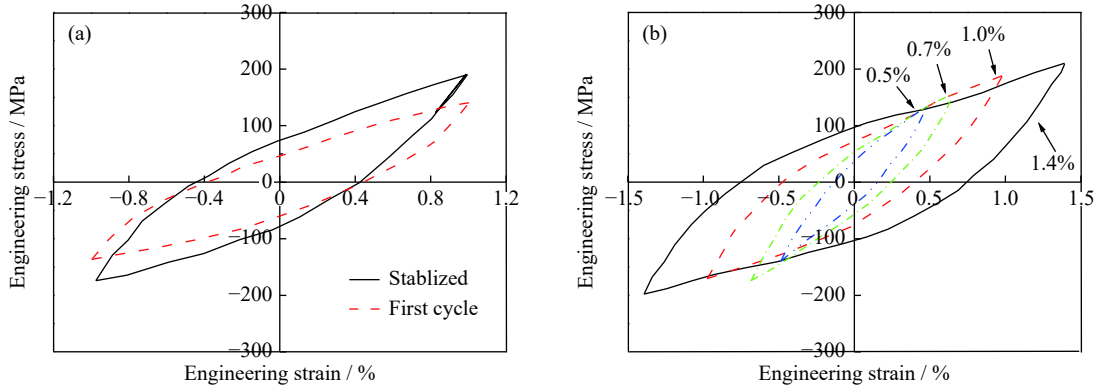

Fig. 3. Stress–strain responses of cast AZ80 Mg alloy in strain-controlled cyclic tests under different strain amplitudes: (a) 1.0%; (b) stabilized responeses under different amplitudes. Reprinted from *Int. J. Fatigue*, 104, A. Gryguc, S.K. Shaha, S.B. Behravesh, H. Jahed, M. Wells, B. Williams, and X. Su, Monotonic and cyclic behaviour of cast and cast-forged AZ80 Mg, 136-149, Copyright 2017, with permission from Elsevier.

ence of strain amplitude on the cyclic plasticity of cast Mg alloys is mainly reflected by different cyclic soft/hardening features, but the strain amplitude has almost no influence on the shape of the stress–strain hysteresis loop (almost symmetrical), different from the case of wrought Mg alloys.

Studies on the cyclic plasticity of cast Mg alloys are not as many as those on the cyclic plasticity of the wrought alloys, especially the studies addressing the effects of strain rate, temperature, and loading path on the cyclic plasticity. Thus, this review focuses on the cyclic plasticity of wrought Mg alloys.

(2) Effects of strain rate.

Begum *et al.* [26] found that stress amplitude responses were almost identical in the fully reversed strain-controlled cyclic tests of extruded AZ31 Mg alloy under a strain amplitude of 0.4% and at different strain rates (i.e., 1×10^{-3}, 1×10^{-2}, and 8×10^{-2} s^{-1}); this means that the influence of strain rate on the stress amplitude response was not significant. However, for the extruded AZ80 Mg alloy, cyclic hardening occurred in the reversed strain-controlled cyclic tests at different strain rates under a strain amplitude of 0.8%, and the extent of cyclic hardening increased with increasing strain rate [27]. Also, Chen *et al.* [28] revealed that the stress–strain hysteresis loops of extruded AZ31B Mg alloy at different strain rates were all asymmetrical, and the strain rate had little effect on the valley stress, but the peak stress increased with increasing strain rate (Fig. 4). This implies that the rate-dependent cyclic plasticities of extruded AZ31B Mg alloy in tension and compression are different, and the rate dependence in tension is much more significant than that in compression.

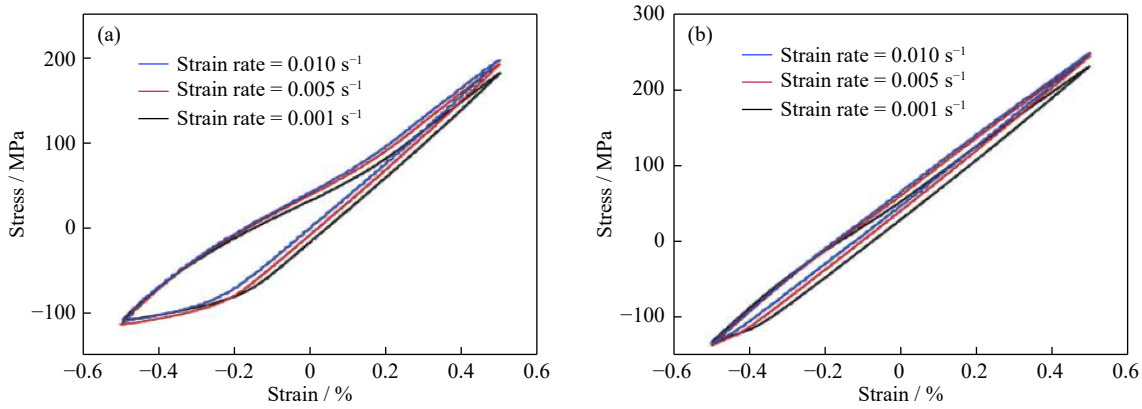

Fig. 4. Stress–strain curves of extruded AZ31B Mg alloy in strain-controlled cyclic tests at different strain rates: (a) in the first loading cycle; (b) in the half-life cycle. Reprinted from *J. Alloys Compd.*, 735, G. Chen, J.W. Gao, Y. Cui, H. Gao, X. Guo, and S.Z. Wu, Effects of strain rate on the low cycle fatigue behavior of AZ31B magnesium alloy processed by SMAT, 536-546, Copyright 2018, with permission from Elsevier.

In summary, strain rate has a significant impact on the cyclic hardening of wrought Mg alloys; the rate-sensitivities of cyclic hardening in the tensile and compressive directions are different, due to different plastic deformation mechanisms, which are addressed in Section 2.2.

(3) Effects of temperature.

Kim *et al.* [29] and Piao *et al.* [30] performed some strain-controlled tension–compression–tension and compression–tension tests of extruded AZ31 Mg alloy at different temperatures and found that unique S-shaped stress–strain curves gradually disappeared as the temperature increased, due to the decrease in the critical resolved shear stresses (CRSSs) of non-basal slip systems. Jiang *et al.* [31] revealed that the extension twin fractions formed in the uniaxial compression of extruded AM30 and AZ31 Mg alloys at different temperatures were very close when the temperature was lower than 200°C, which means that the temperature had little effect on the twinning at relatively lower temperatures. In [29–31], wrought Mg alloys presented different temperature dependencies during plastic deformation involving different physical mechanisms; however, cyclic plasticity and its temperature dependence were not addressed.

Recently, Li *et al.* [10] conducted uniaxial strain-controlled cyclic tests at five temperatures (25, 100, 150, 200, and 250°C) to investigate the temperature-dependent cyclic plasticity of extruded AZ31B Mg alloy. Fig. 5 displays the stress–strain curves obtained in the tension–compression–tension and compression–tension tests under the maximum tensile and compressive strains of 3% and −3%, respectively, and at different temperatures [10]. From the figure, as the temperature increased, the tensile yield stress of extruded AZ31B Mg alloy greatly decreased, while the compressive stress was almost insensitive to the temperature variation; meanwhile, the tension–compression asymmetry became increasingly weaker, and the concave-inward stress–strain curves with inflection points (i.e., the S-shaped curves) gradually transitioned to convex-outward curves. From [10], it can be further observed that the cyclic softening/hardening

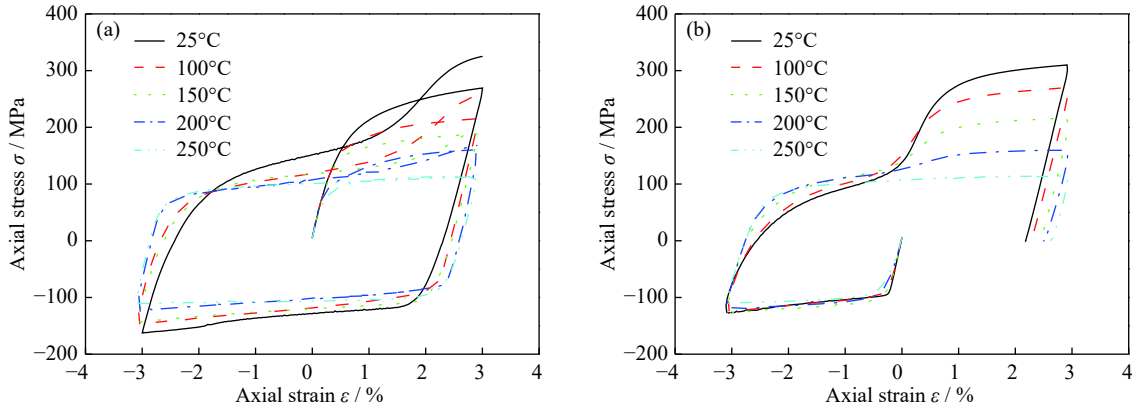

Fig. 5. Stress–strain curves of extruded AZ31B Mg alloy at different temperatures: (a) in tension–compression–tension test; (b) in compression–tension test. Reprinted from *Int. J. Fatigue*, 120, H. Li, G.Z. Kang, C. Yu and Y.J. Liu, Experimental investigation on temperature-dependent uniaxial ratchetting of AZ31B magnesium alloy, 33-45, Copyright 2019, with permission from Elsevier.

features of extruded AZ31B Mg alloy were also dependent on the temperature; that is, at temperatures lower than 150°C, apparent cyclic hardening occurred; but at temperatures higher than 150°C, remarkable cyclic softening occurred.

In summary, wrought Mg alloys exhibit temperature-dependent cyclic softening/hardening because different plastic deformation mechanisms, including the basal and non-basal dislocation slipping and twinning/detwinning, will be activated at different temperatures.

(4) Effects of multiaxial loading.

The multiaxial cyclic plasticity of materials is much more complex than the uniaxial cyclic plasticity. Thus, existing results for the multiaxial cyclic plasticity of wrought Mg alloys are briefly summarized here.

Wang *et al.* [32] revealed that the stress–strain hysteresis loops of extruded GW83 Mg alloys with a random texture were completely symmetrical in fully reversed cyclic torsional tests under torsional strain amplitudes from 0.606% to 4.157%; the shear stress amplitude decreased cyclically (i.e., apparent cyclic softening occurred) under shear strain amplitudes larger than 1.732%, while slight cyclic softening appeared at the early loading stage and then transitioned to cyclic hardening when the shear strain amplitude was larger than 1.732%. Albinmousa *et al.* [12–13] revealed that the axial stress–strain hysteresis loops of extruded AZ31B Mg alloy were symmetrical in proportional axial-torsional combined cyclic tests, similar to the uniaxial stress–strain hysteresis loops, while the loops obtained in the non-proportional axial-torsional cyclic tests were asymmetrical. This means that proportional and non-proportional multiaxial loading paths significantly affected the cyclic plasticity of wrought Mg alloys. However, no significant additional hardening effect occurred in the non-proportional multiaxial cyclic tests of extruded AZ61A Mg alloy [33]; this result was different from those of the tests of face-centered cubic (fcc) and body-centered cubic (bcc) metals, because the slip systems of Mg alloys are so limited and twinning contributes a large amount of plastic deformation. Furthermore, Yu *et al.* [34] demonstrated that non-proportional additional softening/hardening features in axial and torsional directions were not identical in the fully reversed multiaxial strain-controlled cyclic tests of extruded AZ61A Mg alloy, and the axial stress amplitude with a circular path was slightly lower than the corresponding uniaxial stress amplitude at a stabilized cycle, but the torsional stress amplitude with a circular path was much larger than the corresponding pure torsional stress amplitude. Recently, Li *et al.* [35] revealed that the axial and torsional shear stress amplitudes increased cyclically in multiaxial cyclic tests of extruded AZ31 Mg alloy with different loading paths (Fig. 6), which means that remarkable cyclic hardening occurred in both axial and torsional directions.

It can be further revealed from [35] that the axial stress amplitude response in the uniaxial strain-controlled cyclic test is larger than that in the multiaxial ones, which indicates remarkable additional softening in the axial direction; the equivalent shear stress amplitude in the pure torsional test is smaller than that in the multiaxial cyclic tests, which demonstrates a remarkable additional hardening in the torsional direction. Non-proportional multiaxial additional hardening was also observed in [36] and [37] for extruded AM30 and AZ80 Mg alloys, respectively. In summary, the multiaxial strain-controlled cyclic deformation of Mg alloys strongly depends on the loading path, and various plastic deformation mechanisms will make the multiaxial cyclic plasticity of Mg alloys complicated; this phenomenon should be paid much more attention in the future. Overall, remarkable cyclic hardening occurs during the strain-controlled cyclic deformation of wrought Mg alloys and is affected by several factors, such as applied strain amplitudes, temperature, and loading path.

2.1.2. Stress-controlled cyclic deformation

As reviewed by [38–40], ratchetting occurs during the asymmetrical stress-controlled cyclic tests of materials. The ratchetting strain (the average of peak and valley strains) can increase cyclically, and consequently, the geometric size of

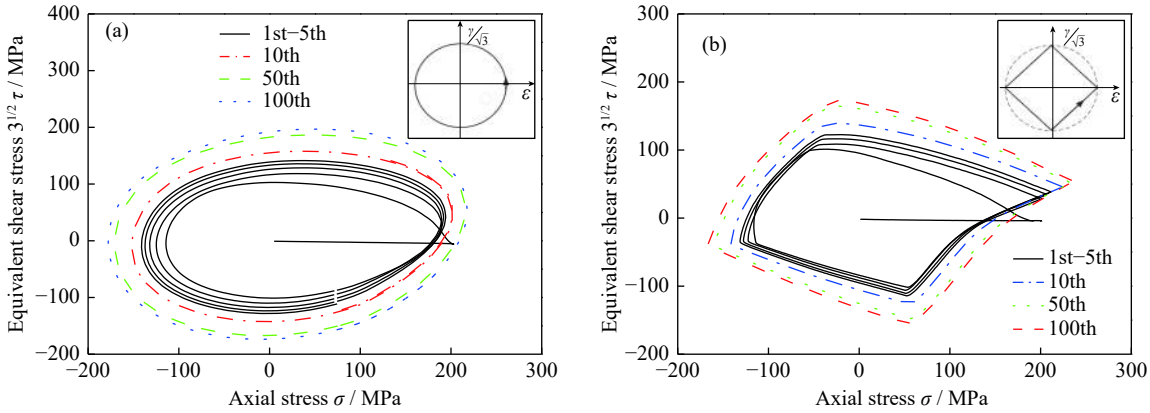

Fig. 6. Axial and shear stress responses of extruded AZ31 Mg alloy in multiaxial strain-controlled cyclic tests with different loading paths: (a) circular path; (b) rhombic path. Reprinted from *Mater. Sci. Eng. A*, 671, H. Li, G.Z. Kang, Y.J Liu, and H. Jiang, Non-proportionally multiaxial cyclic deformation of AZ31 magnesium alloy: Experimental observations, 70-81, Copyright 2016, with permission from Elsevier.

structural components will exceed the design limitation; also, the fatigue life of the materials will significantly reduce, which often results in the premature failure of structures. Therefore, the ratchetting of Mg alloys and its dependences on stress level, stress rate, temperature, and multiaxial loading path are worth investigating. The existing experimental results (only for the wrought alloys) are reviewed as follows:

(1) Effect of stress level.

Xiong *et al.* [9] and Kang *et al.* [41] investigated the stress-level-dependent ratchetting of extruded ZK60 and AZ31 Mg alloys, respectively. The studies showed that significant ratchetting occurred and the ratchetting strain rate (i.e., the increment of ratchetting strain per cycle) decreased cyclically, but its evolution features were different in the cyclic tests of Mg alloys with different mean stresses and stress amplitudes, because of different plastic deformation mechanisms. Typical cyclic stress–strain curves of extruded AZ31 Mg alloy with different mean stresses [41] are presented in Fig. 7 and are addressed in detail as follows:

Fig. 7 shows the following: (1) In the case of (100 ± 110) MPa (i.e., an axial mean stress of 100 MPa and a stress amplitude of 110 MPa), the stress–strain hysteresis loops of extruded AZ31 Mg alloy were symmetrical and always shifted in the tensile direction; significant ratchetting occurred (Fig. 7(a)), like in the cases of traditional fcc and bcc metallic materials [39]. Since the valley stress was much smaller than the alloy compressive yield stress, the cyclic plastic deformation was only dominated by dislocation slipping. (2) In the case of (50 ± 180) MPa, the peak and valley stresses were higher than the alloy tensile and compressive yield stresses, respectively, and then the cyclic plastic deformation was simultaneously dominated by dislocation slipping, twinning, and detwinning. The stress–strain hysteresis loops were asymmetrical, and S-shaped stress–strain curves appeared in the reverse tensile stages (Fig. 7(b)). (3) In the case of (0 ± 120) MPa, the peak stress was smaller than the alloy tensile yield stress. Therefore, the cyclic plastic deformation was simultaneously dominated by twinning and detwinning, and the stress–strain hysteresis loops were asymmetrical in the first five loading cycles but gradually became almost symmetrical in the subsequent cycles. Meanwhile, the evolution trends of the peak strain (shifts in the compressive direction) and valley strain (shifts in the tensile direction) were not identical (Fig. 7(c)). (4) In the case of (−60 ± 80) MPa, the plastic deformation was also controlled by twinning and detwinning, which is similar to the case of (0 ± 120) MPa, but the formed twins could be partially detwinned due to relatively lower peak stress, which resulted in symmetrical and convex hysteresis loops. The peak and valley strains shifted in the compressive direction (Fig. 7(d)).

Furthermore, in [42], significant ratchetting occurred in the stress-controlled cyclic tests of hot-rolled AZ31B Mg alloy when the peak stress was sufficiently large, and the ratchetting strain evolution was divided into three stages (initial rapid growth, stable development, and final steep increase). Also, in [42], the evolution trend of the density of geometrically necessary dislocations was similar to that of ratchetting strain. However, the ratchetting of Mg alloys is only discussed in the tensile direction in [42], which means that no plastic deformation occurred in the compressive direction.

Overall, the stress level determines the activated cyclic plastic deformation mechanism and remarkably influences the shape of the stress–strain hysteresis loop and the evolution trend of ratchetting in wrought Mg alloys.

(2) Effect of stress rate.

Regarding the stress-rate-dependent ratchetting of wrought Mg alloys, it has been concluded that the ratchetting of rolled AZ31B Mg alloy is not sensitive to the change in stress rate (10, 50, and 100 MPa/s) [43]. Moreover, it has been reported that the higher the stress rate, the smaller the ratchetting strain of hot-rolled AZ91D Mg alloy [44]. In [44], the differences in ratchetting strains observed at various

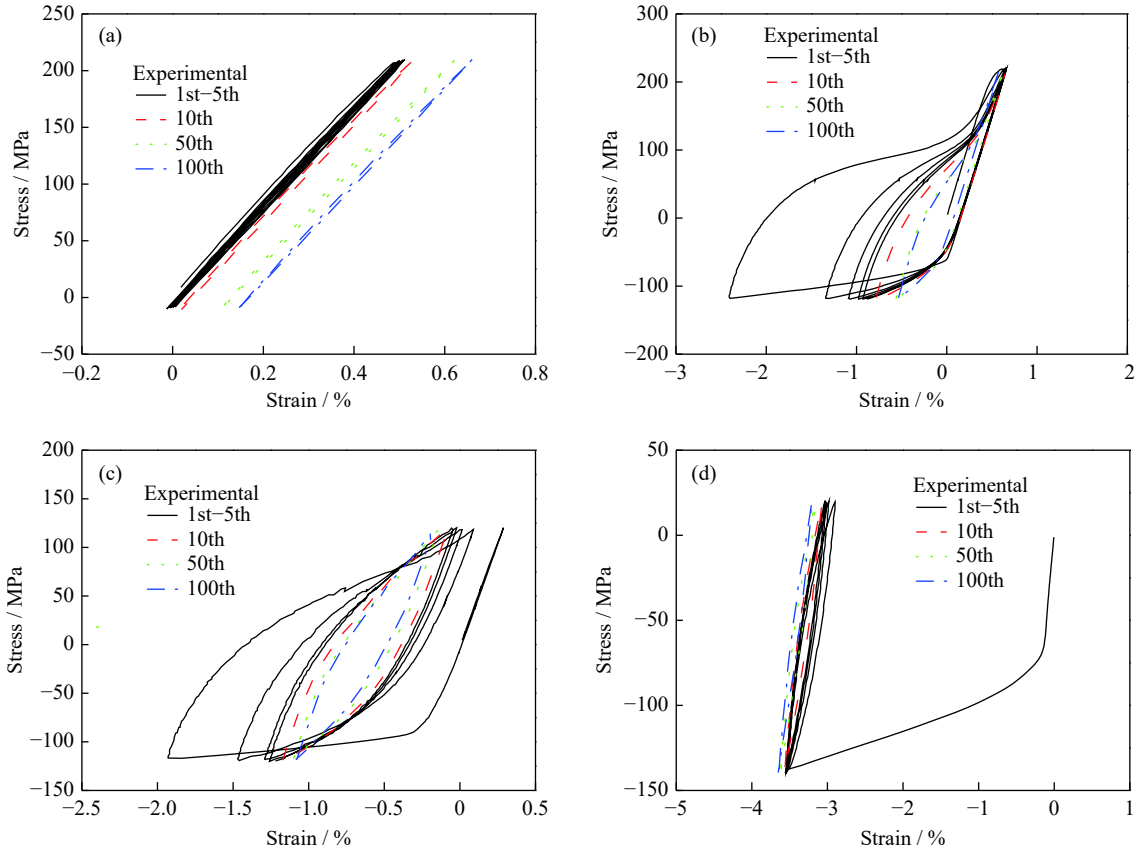

Fig. 7. Stress–strain curves obtained in the stress-controlled cyclic tests of extruded AZ31 Mg alloy with different mean stresses and stress amplitudes: (a) (100 ± 110) MPa; (b) (50 ± 170) MPa; (c) (0 ± 120) MPa; (d) (−60 ± 80) MPa. Reprinted from *Mater. Sci. Eng. A*, 607, G.Z. Kang, Y. Chao, Y.J. Liu, and G.F. Quan, Uniaxial ratchetting of extruded AZ31 magnesium alloy: Effect of mean stress, 318-327, Copyright 2014, with permission from Elsevier.

stress rates occurred in the first cycle of each test, and the subsequent evolution trends of ratchetting were almost the same. In the prescribed tests of rolled Mg alloys in [43–44], the plastic deformation was only dominated by dislocation slipping; no twinning or detwinning occurred, due to the adopted stress levels. Moreover, Meng *et al.* [45] found that the ratchetting of rolled AZ31B Mg alloy was insensitive to the stress rate under the activation of twinning/detwinning.

In summary, the rate dependence of the ratchetting of wrought Mg alloys is controlled by the activated plastic deformation mechanism, but detailed investigations on the rate-dependent ratchetting considering different plastic deformation mechanisms and their interactions are still lacking.

(3) Effect of temperature.

Regarding the temperature-dependent ratchetting of Mg alloys, in [46], it was found that the significant cyclic hardening at lower temperatures transitioned to cyclic softening with the increase in temperature, and significant ratchetting occurred in the stress-controlled cyclic tests of rolled AZ91 Mg alloy at higher temperatures. Recently, Li *et al.* [10] investigated the temperature-dependent ratchetting of extruded AZ31 Mg alloy by performing uniaxial cyclic tests with different peak/valley stresses and at various test temperatures. Fig. 8 displays the evolution curves of ratchetting strain with the number of cycles [10]. The relative peak/valley stresses (multiples of the tensile and compressive yield stresses, σ_y^t and σ_y^c, respectively, of the alloy at various temperatures) were employed to realize a simple and direct comparison of experimental data.

Fig. 8 shows that the ratchetting of extruded AZ31 Mg alloy greatly depended on the test temperature, but the temperature-dependent ratchetting was significantly affected by the adopted stress levels: (1) In the test with a peak stress of $1.1\sigma_y^t$ and a valley stress of $0.2\sigma_y^c$, the ratchetting strain increased with the temperature; however, at 25, 100, and 150°C, the ratchetting strain rate decreased to a constant after certain cycles, and then stable ratchetting occurred. As the temperature reached 200 or 250°C, the ratchetting strain rate continuously increased, and the ratchetting strain significantly accumulated due to the cyclic softening of the alloy (Fig. 8(a)). (2) In the test with a peak stress of $1.1\sigma_y^t$ and valley stress of $1.1\sigma_y^c$, when the temperature was not higher than 150°C, ratchetting apparently occurred, and the peak and valley strains cyclically accumulated in the same tensile direction. When the temperature was 200 or 250°C, the ratchetting strain was almost zero, since the tension–compression

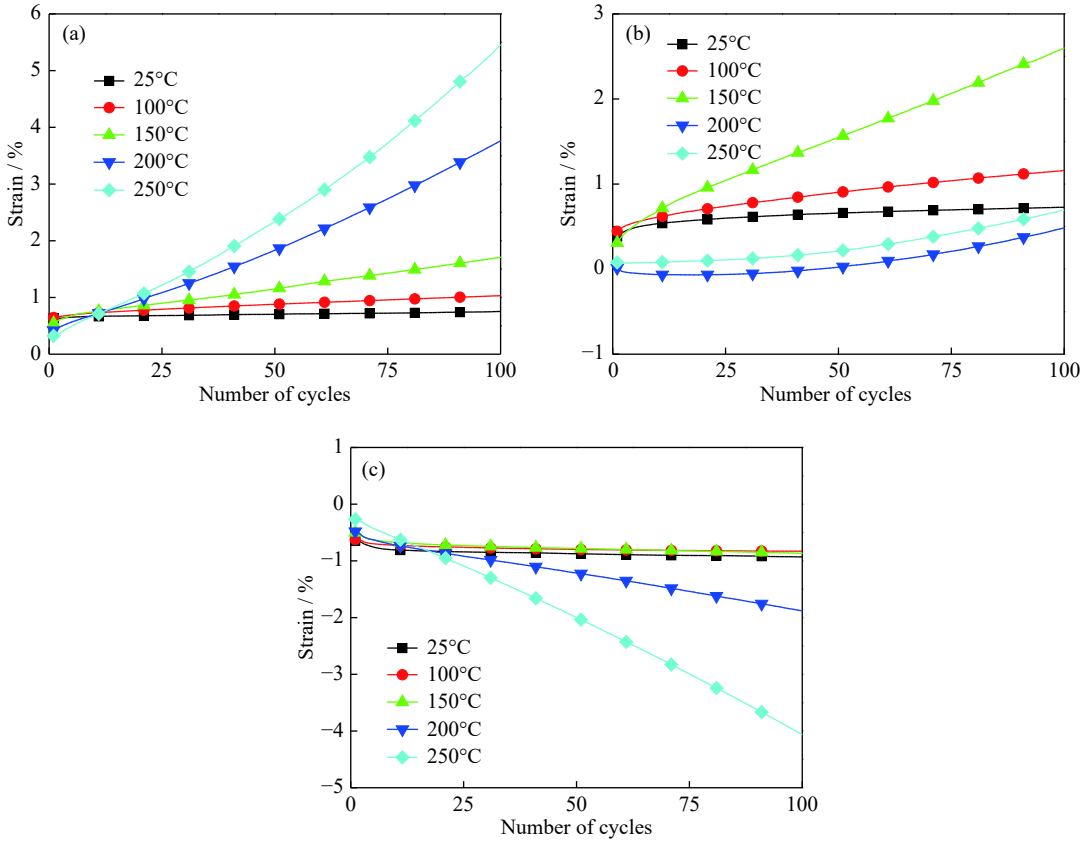

Fig. 8. Curves of ratcheting strain vs. number of cycles for extruded AZ31 Mg alloy at various temperatures: (a) with a peak stress of $1.1\sigma_y^t$ and a valley stress of $0.2\sigma_y^c$; (b) with a peak stress of $1.1\sigma_y^t$ and a valley stress of $1.1\sigma_y^c$; (c) with a peak stress of $0.2\sigma_y^t$ and a valley stress of $1.1\sigma_y^c$. Reprinted from *Int. J. Fatigue*, 120, H. Li, G.Z. Kang, C. Yu and Y.J. Liu, Experimental investigation on temperature-dependent uniaxial ratchetting of AZ31B magnesium alloy, 33-45, Copyright 2019, with permission from Elsevier.

asymmetry of the alloy became very weak at such temperatures (Fig. 8(b)). (3) In the test with a peak stress of $0.2\sigma_y^t$ and valley stress of $1.1\sigma_y^c$, when the temperature was not higher than 150°C, the compressive ratchetting strains were almost the same and were nearly independent of the temperature, due to twinning being the only activated deformation mechanism; however, when the temperature was 200 or 250°C, much more significant ratchetting than those at 25, 100, and 150°C occurred, and the ratchetting strain increased in the compressive direction at a constant rate after certain cycles (Fig. 8(c)).

In summary, the ratchetting of wrought Mg alloys is significantly temperature-dependent, and the temperature-dependent ratchetting is also related to the applied stress levels, due to the activation of different plastic deformation mechanisms in the compressive and tensile directions.

(4) Effects of multiaxial loading.

The multiaxial loading paths have a great influence on the ratchetting of materials, as reviewed by [39]; thus, it is necessary to address their impact on the ratchetting of wrought Mg alloys. However, existing studies on the multiaxial ratchetting of Mg alloys are not as sufficient as those on the uniaxial ratchetting. Castro and Jiang [47] investigated the ratchetting of extruded AZ31B Mg alloy in both the axial and shear directions by performing a multiaxial (combined tension-torsion) stress-controlled cyclic test with a circular path. They found that the axial ratchetting was more significant than the torsional ratchetting. Recently, Li *et al.* [35] investigated the non-proportional multiaxial ratchetting of extruded AZ31 Mg alloy with different loading paths and at room temperature. Figs. 9(a) and 9(b) demonstrate the axial and torsional strain responses in the cases with circular and rhombic paths, where the axial stress level was (100 ± 120) MPa and the equivalent shear level was (0 ± 120) MPa. The results with an axial stress level of (−20 ± 120) MPa are displayed in Figs. 9(c) and 9(d).

Fig. 9 shows that ratchetting occurred in the axial direction and that the axial ratchetting strain increased cyclically, whereas, no significant ratchetting occurred in the shear direction. Meanwhile, the multiaxial ratchetting of the extruded AZ31 Mg alloy depended on the shapes of the loading paths and the magnitude of the axial mean stress, and it evolved in the compressive direction when a negative axial mean stress was adopted.

The evolutions of the axial and uniaxial ratchetting strains obtained in [35] under different loading paths and a positive axial mean stress (Fig. 10(a)) revealed that the axial ratchet-

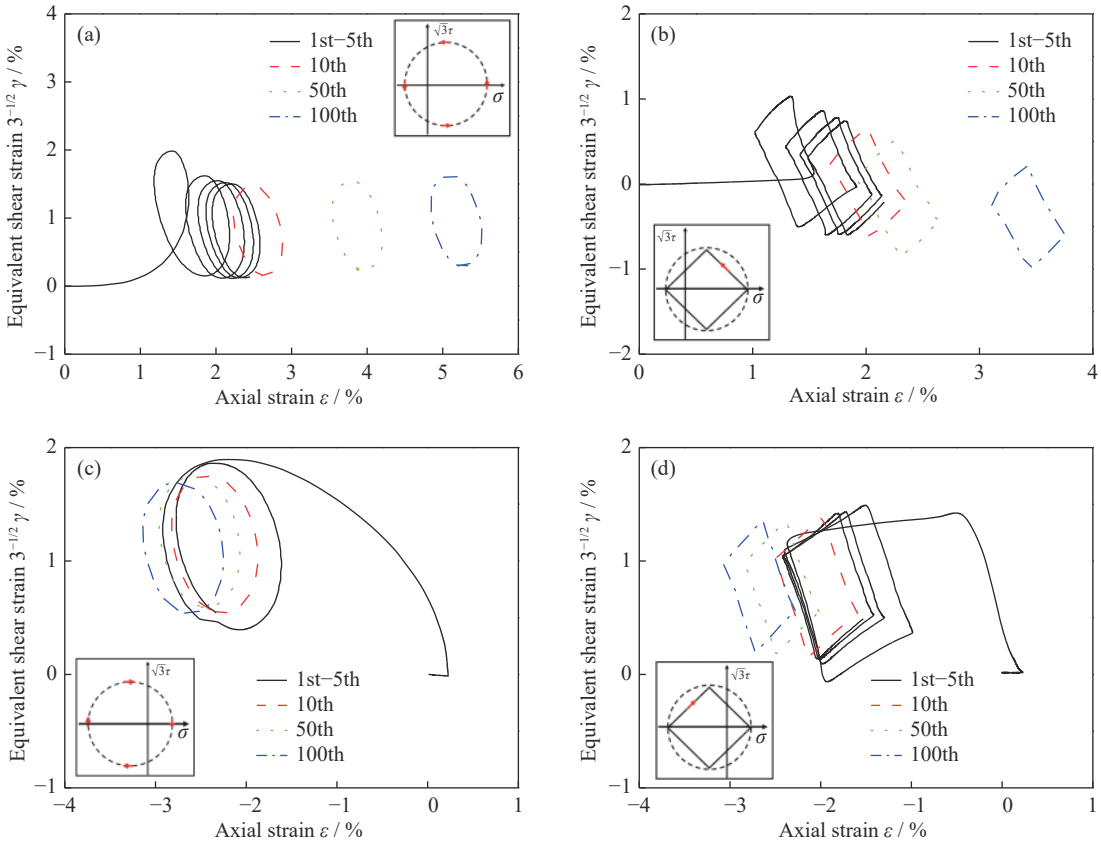

Fig. 9. Axial and torsional strain responses of AZ31 Mg alloy in multiaxial cyclic tests: (a) an axial stress level of (100 ± 120) MPa with circular path; (b) an axial stress level of (100 ± 120) MPa with rhombic path; (c) an axial stress level of (−20 ± 120) MPa with circular path; (d) an axial stress level of (−20 ± 120) MPa with rhombic path. Reprinted from *Mater. Sci. Eng. A*, 671, H. Li, G.Z. Kang, Y.J Liu, and H. Jiang, Non-proportionally multiaxial cyclic deformation of AZ31 magnesium alloy: Experimental observations, 70-81, Copyright 2016, with permission from Elsevier.

ting strains with non-proportional multiaxial circular and rhombic paths were higher than those with uniaxial and linear paths. Moreover, the evolution curves corresponding to negative axial mean stress (Fig. 10(b)) showed that significant ratchetting also occurred in the compressive direction, and the ratchetting strains with circular and rhombic paths were close to the uniaxial ratchetting strains, different from the case of the strains under positive axial mean stress (Fig. 10(a)).

In summary, the multiaxial ratchetting of wrought Mg alloys strongly depends on the shapes of loading paths. However, existing studies on the multiaxial ratchetting of Mg

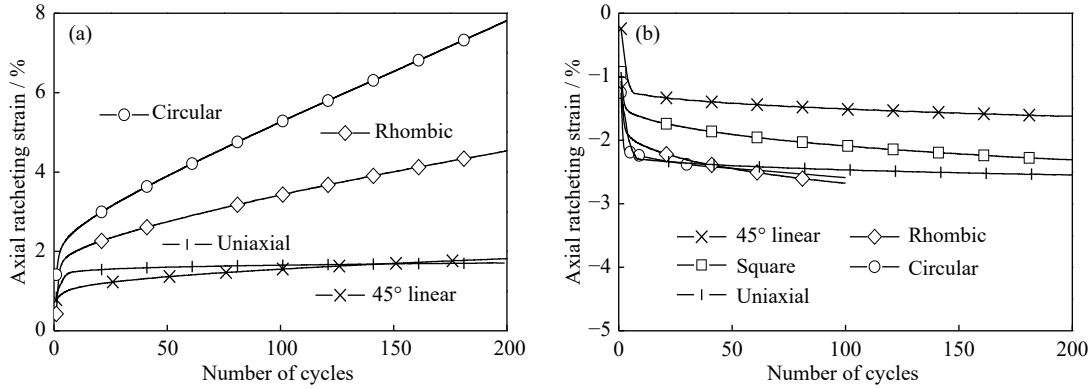

Fig. 10. Evolution curves of axial ratcheting strain of extruded AZ31 Mg alloy in cyclic tests with various loading paths: (a) an axial stress level of (100 ± 120) MPa; (b) an axial stress level of (−20 ± 120) MPa. Reprinted from *Mater. Sci. Eng. A*, 671, H. Li, G.Z. Kang, Y.J Liu, and H. Jiang, Non-proportionally multiaxial cyclic deformation of AZ31 magnesium alloy: Experimental observations, 70-81, Copyright 2016, with permission from Elsevier.

alloys are mostly concentrated in the ratchetting in the axial direction, that is, with a non-zero axial and zero torsional mean stresses. The multiaxial ratchetting of Mg alloys in both axial and torsional directions has not yet been investigated. Experimental studies on the multiaxial ratchetting of Mg alloys should be systematically conducted by considering the effects of stress level, stress rate, and test temperature.

2.2. Microscopic observations

Although some explanations have been offered for the cyclic plasticity of Mg alloys based on plastic deformation mechanisms, including dislocation slipping, twinning, and detwinning, the microscopic details of dislocation slipping and twinning and their interaction cannot be revealed by macroscopic tests. Therefore, it is important to profoundly understand the dislocation slipping, twinning, and detwinning and their interactions by microscopic observations. Here, the progress in the microscopic observations on the plastic deformation mechanism of Mg alloys is summarized as follows: first, dislocation slipping, including that in basal, prismatic, and pyramidal slip systems, is summarized; then, the initiation and development of twinning and detwinning are discussed; finally, the interactions are addressed.

2.2.1. Dislocation slipping in Mg alloys

The slip systems in Mg alloys include the basal, prismatic, and pyramidal slip systems [48−50], and the basal slip (dislocation slipping in basal slip systems) is the most easily activated plastic deformation mechanism. Based on the experiments of Mg single crystals, the CRSS of basal slip at room temperature is estimated to be only about 0.5 MPa; however, only two independent slip systems can be provided. Therefore, although the basal slip is the most easily activated deformation mechanism, it cannot accommodate arbitrary plastic deformation, according to the von Mises' uniform deformation criterion. The prismatic slip system is another common slip system in Mg alloys, but its CRSS is much higher than that of the basal slip at room temperature (usually by two orders of magnitude); therefore, it is difficult to be activated. Concerning the prismatic slip (dislocation slipping in prismatic slip systems), only two independent slip systems can also be provided. Both the basal and prismatic slips are accompanied by the <a> dislocations, whose slip directions are parallel to the basal plane, and they cannot accommodate the plastic deformation of the alloys along the *c*-axis. Thus, the pyramidal slip (dislocation slipping in the pyramidal slip system) is significant for accommodating the plastic deformation of wrought Mg alloys. The progress in the activation and development of pyramidal slip in the Mg alloys is briefly summarized as follows:

Several studies [49−56] have demonstrated that the dislocations involved in the pyramidal slip of Mg single crystals can be classified into two types: <a> and <c+a> dislocations. The pyramidal <a> dislocation slip can occur in four independent slip systems, but from a crystallographic viewpoint, it can be regarded as the result of the joint action of basal and prismatic slip systems; no new independent slip systems are provided. Therefore, the pyramidal <c+a> dislocation slip is more important than the pyramidal <a> one. The pyramidal <c+a> dislocation lies in and can glide on either the $\{10\bar{1}1\}$ pyramidal I or $\{11\bar{2}2\}$ pyramidal II slip plane, but the characteristics of these two dislocation structures and their activation energies are different. The pyramidal <c+a> dislocation slip can accommodate the plastic deformation along the *c*-axis of Mg crystals. However, the pyramidal <c+a> dislocation slip is hard to be activated due to its poor mobility. Nevertheless, Stohr and Poirier [51], Obara *et al.* [52], and Ando *et al.* [53] confirmed the existence of pyramidal <c+a> dislocation in Mg single crystals through transmission electron microscopy (TEM) observations; Lilleodden [54], Byer *et al.* [55], and Xie *et al.* [56] observed the pyramidal slip in compressive experiments of Mg single-crystal. In the above-mentioned studies, many observed dislocations were the <a>-type dislocations and non-basal dislocations, but the dislocations in the *c*-axis direction were rare.

However, the above-mentioned dislocation structures were all observed after the monotonic deformation. The generation and movement of dislocations during the cyclic deformation of Mg alloys were more complicated. Guillemer *et al.* [57] observed the microstructure of pure polycrystalline Mg after cyclic deformation under a plastic strain amplitude of 0.1% by TEM and found that the basal, prismatic, and pyramidal <a> slips appeared near the grain or twin boundary.

In summary, the pyramidal slip of Mg alloys is relatively complex, and the local stress concentration caused by the twins or by the dislocation pile-up during the cyclic deformation of Mg alloys may affect the activation and motion of pyramidal slips; therefore, it is necessary to systematically investigate the dislocation structures and their evolutions at different stages of cyclic plastic deformation and clarify the activation and evolution of dislocation slipping.

2.2.2. Twinning and detwinning in Mg alloys

Regarding twinning in Mg alloys, there are many microscopic experimental results, which cannot be fully discussed in this review due to space limitations. Thus, only some typical and representative results are addressed here; others can be found in the references therein.

Lou *et al.* [7] observed the evolution of twin volume fraction in a compression–tension test of rolled AZ31B Mg alloy via optical microscopy. As shown in Fig. 11, f_{twin} is the twin volume fraction, many twins occurred in the compressive stage, and the generated twins were gradually detwinned in the reverse tensile stage.

Wu *et al.* [58] and other researchers [59−60] observed the twinning and detwinning from different scales using *in situ* synchrotron X-ray imaging and diffraction. They found that

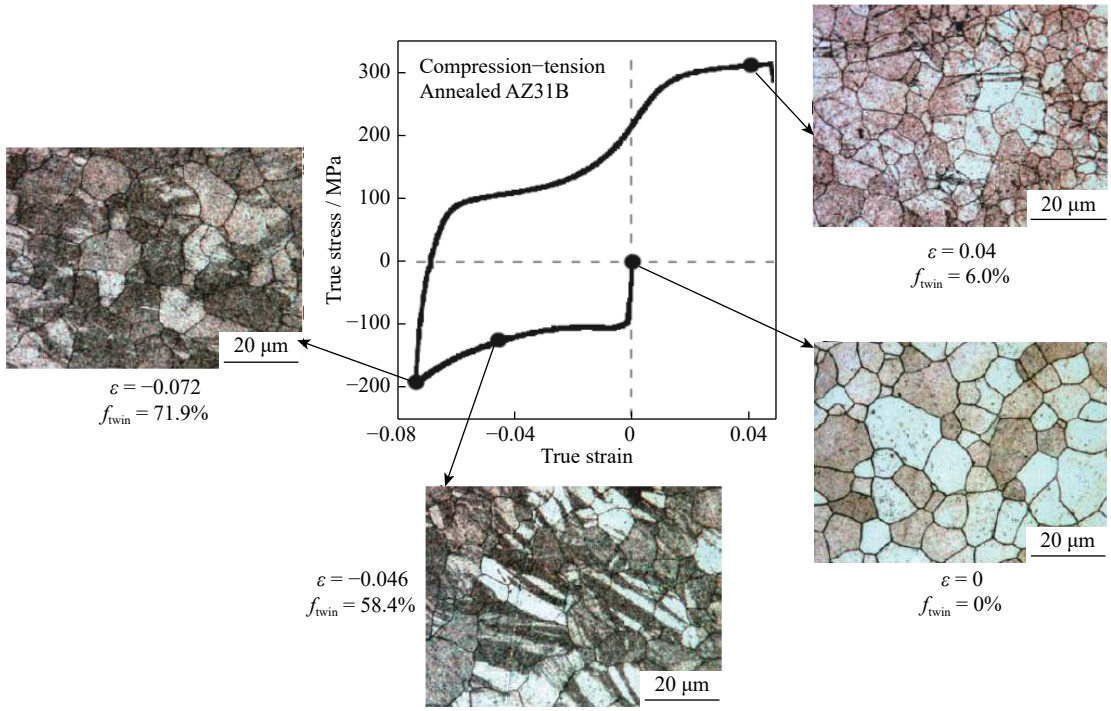

Fig. 11. Evolution of twin volume fraction in the compression–tension test, as observed by optical microscopy. Reprinted from *Int. J. Plast.*, 23, X.Y. Lou, M. Li, R.K. Boger, S.R. Agnew, and R.H. Wagoner, Hardening evolution of AZ31B Mg sheet, 44-86, Copyright 2007, with permission from Elsevier.

significant decrease in lattice strain occurred in the parent grains on both sides of the twin, as the plastic deformation was dominated by twinning, but little change in lattice strain occurred as the plastic deformation was dominated by detwinning. In addition, a reorientation process such as twinning in the grain appeared in the deformed Mg alloy.

In addition, TEM and electron backscatter diffraction (EBSD) were employed to observe the microstructure evolution during the cyclic deformation [18,61]. For example, Dong *et al.* [61] investigated the twinning and detwinning in the cyclic deformation of extruded ZK60 Mg alloy after specific cycles by EBSD and found that the formed twins in the grains in the compressive stage were mostly parallel to each other or existed as only one twin per grain. Dong *et al.* [18] also explored the evolution of twin morphology and volume fraction in the extruded ZK60 Mg alloy after different cycles. They found that the difference in twin volume fractions at the peak and valley stresses in each cycle decreased cyclically, which means that the activities of twinning and detwinning also reduced cyclically. Yin *et al.* [62] further confirmed the occurrence of twinning and detwinning in the cyclic deformation of extruded AZ31 Mg alloy by *in situ* EBSD. Yu *et al.* [63] observed the microstructures of Mg single-crystal after cyclic tests in [0001] and [10$\bar{1}$0] directions, investigated two types of twin–twin interactions with different crystallographic orientations, and concluded that the twin–twin boundary hindered the detwinning. Sun *et al.* [64] also found that the detwinning was hindered by multiple twin variants appearing in the grains. Furthermore, Wu *et al.* [65] found from an *in situ* neutron diffraction observation that the internal tensile residual stress generated in extruded ZK60 Mg alloy during twinning could drive the detwinning in the reversal tensile stage. Sarker *et al.* [66] also revealed that the twins in the extruded AM30 Mg alloy increased with increasing compressive pre-strain, but the detwinning activity decreased.

In summary, twinning is an important plastic deformation mechanism of Mg alloys, and it can accommodate a certain amount of plastic deformation and cause the rotation of twinned grains. Thus, it is necessary to investigate the evolution of twin volume fraction, distribution, and morphology during the cyclic plasticity of Mg alloys; study the activation and evolution of formed twins; and reveal the microscopic mechanism involved.

2.2.3. Interactions between dislocations and twins

In Mg alloys, besides the most common dislocation–dislocation interactions, the activation of twinning makes the plastic deformation more complicated: The twinning results in lattice rotation with a large angle; this induces changes in the orientations of slip systems in the twinned region, and the twin boundary significantly reduces the mean free path of dislocation slipping, resulting in the Hall–Petch hardening effect. The twin boundary further acts as a barrier to the movement of subsequent dislocation slipping. Also, the dislocations can react with twin boundary in terms of dislocation transmutations; the dislocation-induced local stress field

in the alloys further affects subsequent nucleation position and the propagation morphology of twins. Thus, it is necessary to investigate the interaction between the dislocation slipping and twinning/detwinning.

About the interaction between the dislocation slipping and twinning, in [67], the microscopic observations by *in situ* TEM showed that dislocations increased cyclically, which may act as a barrier to the propagation of twins, or as a preferential site for twins nucleation in a rolled Mg plate. In [68], when the compressive strains along the ED were below 2.7%, the dislocation-associated mechanism was the main strain hardening mechanism in an extension twinning–predominant deformation of extruded Mg alloys. As the compressive strain increased, the strain hardening from both dislocations and extension twins increased. In addition, Ma *et al.* [69] found that the rapid hardening occurred in the tensile reversal of extruded AM30 Mg alloy, which was caused by the dislocations in the twins. Dong *et al.* [70] revealed that dislocation slipping promoted the twin nucleation but suppressed the growth and shrinkage of twins. Chen *et al.* [71] found that the dislocation slipping caused by the pre-strain (5% and 10%) suppressed the nucleation of extension twin but had little effect on the twin growth of extruded AZ31B Mg alloy. Yu *et al.* [72] found that the existing extension twins had different hindrances to the basal and pyramidal slips of rolled AZ31 Mg alloy, and the hindrance to the basal slip was more remarkable. Jeong *et al.* [73] revealed that when twins were formed, the basal slip within them would be activated to release accumulated strain energy.

Existing studies show that some dislocation reactions with an extension twin boundary will occur. For example, Yoo [74] analyzed the interaction between four different twin variants and dislocations and found that the interaction between basal dislocation and extension twin boundary was repellent, meaning that the incorporation of such dislocations was energetically unfavorable. Wang and Agnew [75] observed that the basal <a> dislocations in the matrix of rolled AZ31 Mg alloy would be transformed into <c+a> ones in the extension twins. Wang *et al.* [76−77] further showed that a transmutation reaction of <a> dislocation in the matrix occurred when the <a> dislocation encountered the twin boundary, and then it decomposed in the twin to produce <c> dislocations.

In summary, complicated interaction between the dislocation slipping and twinning/detwinning has been observed in Mg and its alloys, which is affected by various factors, such as the morphology, distribution, and volume fraction of twins, and becomes more complicated in the cyclic plasticity. Furthermore, some studies [78−83] have reasonably demonstrated the effects of grain boundary and strong basal texture on the dislocation slipping, twinning, and detwinning; however, the complex interaction among them has not yet been clarified. Thus, a great challenge still exists in the physical mechanism studies on the cyclic plasticity of Mg alloys.

3. Constitutive models

As discussed in Section 2, multiple plastic deformation mechanisms and their complex interactions occur during the cyclic deformation of Mg alloys, which increases the difficulty in constructing cyclic constitutive models. Reasonable modeling of the above-mentioned multi-physical processes and their interactions becomes very vital. The physical phenomena reviewed in Section 2 can be reasonably described by the macroscopic phenomenological and crystal plasticity-based constitutive models, which are the two most common constitutive models describing the cyclic plasticity of the wrought Mg alloys and are reviewed here.

3.1. Phenomenological constitutive models

Although macroscopic phenomenological constitutive models cannot directly reveal the microstructure evolution during the plastic deformation of materials, they are widely used in the structural analysis because of their low computational cost and easy implementation into a finite element code. Therefore, the construction of phenomenological constitutive models is an important issue in modeling the cyclic plasticity of Mg alloys, and valuable results have been obtained thus far, some of which will be reviewed here. As mentioned above, during the cyclic plastic deformation of wrought Mg alloys, strong anisotropy and tension–compression asymmetry occur because of the polar nature of twinning and strong basal texture. The traditional von Mises' yield criterion is no longer applicable and should be extended. The established phenomenological constitutive models of Mg alloys can be roughly classified into three groups: (1) von Mises' yield criterion-based models [84−87], where various kinematic and isotropic hardening rules considering different plastic deformation mechanisms are adopted; (2) the Cazacu–Plunkett–Barlat yield criterion-based models [88−94], which adopt different isotropic hardening rules; (3) models based on other yield criteria [95−99]. However, only the first two groups are introduced briefly in the following subsections, and the details about the third group can be found in [95−99].

3.1.1. von Mises' yield criterion-based constitutive models

The von Mises' yield criterion-based models adopt kinematic and/or isotropic hardening rules. For example, Nguyen *et al.* [84] considered three plastic deformation mechanisms of Mg alloys (dislocation slipping, twinning, and detwinning) and separately used three von Mises' yield criteria and isotropic hardening rules to simulate the cyclic plasticity of rolled AZ31B Mg alloy sheet. Lee *et al.* [85] adopted a similar method to simulate the tension–compression–tension deformation of rolled AZ31BMg alloy at different temperatures. Roostaei *et al.* [86] described the anisotropic plasticity

of wrought Mg alloys by introducing a macroscopic plastic modulus into the adopted kinematic hardening rule and simulated the proportional and non-proportional multiaxial cyclic plasticity of extruded AM30, AZ31B, and AZ61A Mg alloys. Li *et al.* [87] proposed a constitutive model based on three plastic deformation mechanisms of rolled AZ31B Mg alloy, called the "TWINLAW" model, and employed the von Mises' yield criterion with an initial non-zero back stress to consider the asymmetric plasticity. Since the TWINLAW model [87] reasonably considers the relationship between the microscopic plastic deformation mechanisms and texture in wrought Mg alloys, it is briefly summarized as follows:

Because different kinematic hardening rules are used in the TWINLAW model to describe various plastic deformation mechanisms of Mg alloys, the relationship between the back stress and texture evolution can be obtained. First, the yield criterion is expressed as

$$f(\boldsymbol{\sigma},\boldsymbol{\alpha}) = \bar{\sigma}(\boldsymbol{\sigma}-\boldsymbol{\alpha}) - \hat{\sigma} = 0 \tag{1}$$

where $\boldsymbol{\sigma}$ and $\boldsymbol{\alpha}$ are Cauchy stress and back stress, respectively, $\bar{\sigma}$ is the equivalent stress, and $\hat{\sigma}$ is the yield surface size. The initial back stress is non-zero due to the anisotropy of Mg alloys and is determined by the initial yield stresses in the tensile and compressive directions. Based on the modified Armstrong–Frederick kinematic hardening rule, three incremental forms of back stress evolution laws are proposed in [87] to separately consider the contributions of dislocation slipping, twinning, and detwinning. For the dislocation slipping mode, the incremental form of back stress is

$$\Delta\boldsymbol{\alpha}' = \Delta\bar{\varepsilon}^{\mathrm{p}}\left(\boldsymbol{B}'_{\mathrm{S}} - \frac{\boldsymbol{\alpha}'_{\mathrm{dif}}}{q}\right) \tag{2}$$

where $\Delta\bar{\varepsilon}^{\mathrm{p}}$ is the equivalent plastic strain increment, $\boldsymbol{\alpha}'_{\mathrm{dif}} = \boldsymbol{\alpha}' - \boldsymbol{\alpha}'_0$, $\boldsymbol{\alpha}'_0$ is the non-zero initial back stress deviatoric tensor, q is a material constant, and $\boldsymbol{B}'_{\mathrm{S}}$ is the second-order deviatoric tensor associated with the dislocation slipping.

The incremental form of back stress for the twinning is

$$\Delta\boldsymbol{\alpha}' = \Delta\bar{\varepsilon}^{\mathrm{p}}\left(\boldsymbol{B}'_{\mathrm{T}} - \frac{\Delta\varepsilon_{\mathrm{c}}^{\mathrm{p}}}{\varepsilon_{\mathrm{twin}}\Delta\bar{\varepsilon}^{\mathrm{p}}}\boldsymbol{\alpha}'\right) \tag{3}$$

where $\varepsilon_{\mathrm{twin}}$ is a constant (0.129) representing the eigen-strain of twinning in Mg alloys, $\Delta\varepsilon_{\mathrm{c}}^{\mathrm{p}}$ is the plastic strain increment in the c-axis direction, and $\boldsymbol{B}'_{\mathrm{T}}$ is the second-order deviatoric tensor associated with the twinning.

The incremental form of back stress for the detwinning is

$$\Delta\boldsymbol{\alpha}' = \Delta\bar{\varepsilon}^{\mathrm{p}}\left(\boldsymbol{B}'_{\mathrm{U}} - \frac{\left|\Delta\varepsilon_{\mathrm{c}}^{\mathrm{p}}\right|}{\varepsilon_{\mathrm{untwin}}\Delta\bar{\varepsilon}^{\mathrm{p}}}\boldsymbol{\alpha}'_{\mathrm{dist}}\right) \tag{4}$$

where $\varepsilon_{\mathrm{untwin}}$ is a constant representing the eigen-strain of detwinning, $\boldsymbol{\alpha}'_{\mathrm{dist}}$ is a linear function of back stress deviatoric tensor $\boldsymbol{\alpha}'$, and $\boldsymbol{B}'_{\mathrm{U}}$ represents the second-order deviatoric tensor associated with the detwinning.

The $\boldsymbol{B}'_{\mathrm{S}}$, $\boldsymbol{B}'_{\mathrm{T}}$, and $\boldsymbol{B}'_{\mathrm{U}}$ are determined by the current texture of the material. The texture evolution is considered, and different hardening laws corresponding to different deformation mechanisms are also proposed based on the macroscopic phenomenological constitutive model. Fig. 12 gives the simulated and experimental stress–strain curves of rolled AZ31B Mg alloy presented in compression–tension–compression and tensile–compression, and the asymmetry and S-shaped stress–strain curves were reasonably simulated by the TWINLAW model. However, much more experimental data in different loading regimes are required to obtain the expressions of flow stresses within different regimes. In addition, the plastic deformation mode should be determined by the plastic strain increment, which means that the cyclic plasticity of Mg alloy can be simulated by the proposed model under a specific loading condition.

3.1.2. Cazacu–Plunkett–Barlat yield criterion-based constitutive models

Unlike in Section 3.1.1, the isotropic von Mises' yield criterion is completely abandoned in the constitutive models

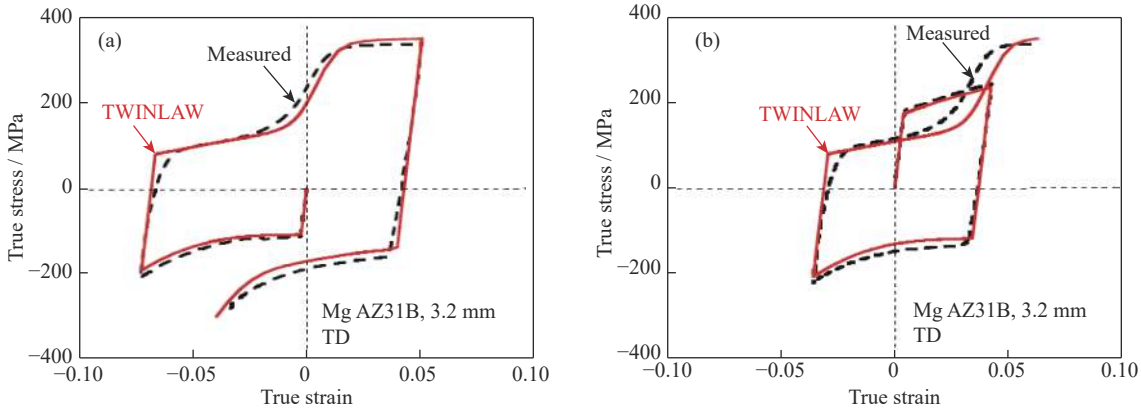

Fig. 12. Simulated and experimental stress–strain curves of AZ31B Mg alloy: (a) compression–tension–compression; (b) tension–compression–tension. Reprinted from *Int. J. Plast.*, 26, M. Li, X.Y. Lou, J.H. Kim, and R.H. Wagoner, An efficient constitutive model for room-temperature, low-rate plasticity of annealed Mg AZ31B sheet, 820-858, Copyright 2010, with permission from Elsevier.

discussed in this subsection, but an anisotropic yield criterion is adopted to describe the plasticity of Mg alloys. First, Cazacu and Barlat [88] proposed a yield criterion reflecting the initial tension–compression asymmetry of Mg alloys by considering the second and third invariants of the stress tensor. Then, Cazacu *et al.* [89] and researchers [90–91] further proposed a yield criterion describing the orthotropic properties of Mg alloys by a linear transformation of the stress deviatoric tensor. A new form of yield criterion developed by Cazacu and Barlat [88] is

$$(|S_1|-kS_1)^a+(|S_2|-kS_2)^a+(|S_3|-kS_3)^a=F \tag{5}$$

where S_1, S_2, and S_3 are three principal values of the stress deviatoric tensor; F is the yield surface size; k is a material constant; and a is a positive integer (usually equal to 2). Eq. (5) is a homogeneous function of principal stresses in an order of a (usually a second-order homogeneous function). According to the proposed criterion in Eq. (5), the ratio of uniaxial tensile yield stress to the compressive stress is given by

$$\frac{\sigma_T}{\sigma_C}=\left\{\frac{\left(\frac{2}{3}\cdot(1+k)\right)^a+2\cdot\left(\frac{1}{3}\cdot(1-k)\right)^a}{\left(\frac{2}{3}\cdot(1-k)\right)^a+2\cdot\left(\frac{1}{3}\cdot(1+k)\right)^a}\right\} \tag{6}$$

The above yield criterion degenerates to the classic von Mises' yield criterion when $a=2$ and $k=0$.

To describe the tension–compression asymmetry and orthotropy of sheet metals, Cazacu *et al.* [89] and reserchers [90–91] extended the above yield criterion as follows:

$$(|\Sigma_1|-k\cdot\Sigma_1)^a+(|\Sigma_2|-k\cdot\Sigma_2)^a+(|\Sigma_3|-k\cdot\Sigma_3)^a=F \tag{7}$$

where Σ_1, Σ_2, and Σ_3 are three principal values of $\boldsymbol{\Sigma}$, and $\boldsymbol{\Sigma}$ is a transformed tensor (its definition can be found in [89]).

The Cazacu–Plunkett–Barlat (CPB) yield criterion is adopted in [89] to effectively describe the anisotropic yielding of Mg alloys. Recently, based on the CPB yield criterion, many phenomenological constitutive models have been established, through which the plastic deformation of Mg alloys could be reasonably described. For example, Yoon *et al.* [92] established a constitutive model to reasonably describe the plasticity of AZ31 Mg alloy by using the Cazacu–Barlat yield criterion combined with a non-associated plastic flow if the *r*-value anisotropy is considered. Tari *et al.* [93] and Muhammad *et al.* [94] investigated the effect of plastic strain on the CPB initial yield criterion and extended it to model the subsequent yielding. Then, they described the anisotropy and asymmetric yielding of wrought Mg alloys.

Although the above-mentioned CPB yield criterion describes the anisotropic deformation of Mg alloys, a large amount of experimental data is required for fitting the parameters, since the linear transformation tensor is a fourth-order tensor related to the accumulated plastic deformation. In addition, the applicability of the CPB yield criterion to the anisotropic cyclic plasticity of Mg alloys needs further verification, especially for the case whereby different plastic deformation mechanisms are involved.

3.2. Crystal plasticity-based constitutive models

A crystal plasticity-based constitutive model is first built on the scale of single-crystal, and then different plastic deformation mechanisms are introduced into the plastic flow rule through the determined crystallographic orientation relationship. Then, full-field solution methods (such as the finite element method) or mean-field approaches (such as Taylor's [100] and self-consistent ones [101–102]) are used to extend the single-crystal model to a polycrystalline model. This type of constitutive model can easily reflect different plastic deformation mechanisms and effectively correlate the macroscopic mechanical response with corresponding microstructures of crystalline materials. Thus, it is more advantageous in the simulation of the cyclic plasticity of crystalline materials with multiple plastic deformation mechanisms than any phenomenological constitutive model. Some crystal plasticity-based constitutive models have been established to describe the plastic deformation of Mg alloys.

The basic problem in modeling the plastic deformation of Mg alloys by the crystal plasticity theory is how to describe the initiation and development of twinning/detwinning, especially for the lattice reorientation caused by the twinning/detwinning. First, Van Houtte [103] developed a statistical model for describing the twinning in the framework of crystal plasticity, where the reorientation occurred once the volume fraction of twins reached a critical value, represented by a pseudo-random number between 0.3 and 1. Tomé *et al.* [104] discussed the shortcomings of Van Houtte's statistical model and proposed a predominated twin reorientation (PTR) method to determine the activated twinning systems by assuming that the twinning only occurred in the most active twinning system (i.e., the one with the largest resolved shear stress (RSS)). Subsequently, Lebensohn and Tomé [105] adopted a more reasonable volume fraction transfer (VFT) approach by hypothesizing that all twinning systems could be simultaneously activated, and the effect of each twinning system on the texture evolution was considered. The VFT method more closely reflects the real physical process of plastic deformation than the PTR method; these two methods have been used in constitutive models describing the twinning of Mg alloys [106–109].

The above-mentioned studies provide a solid theoretical basis for constructing the crystal plasticity-based constitutive models of polycrystalline Mg alloys. However, a transition rule should be used to calculate the overall response of polycrystalline materials from that of single-crystal grain. Thus far, the self-consistent homogenization scheme, finite element method, and explicit scale-transition rule have been commonly used to extend the single-crystal model to a poly-

crystalline one. Because the finite element method is relatively straightforward [110–116], the relevant studies are summarized only in terms of self-consistent homogenization schemes and explicit scale-transition rule.

3.2.1. Models based on self-consistent homogenization scheme

Kröner [101] and Budianski and Wu [102] proposed a self-consistent homogenization scheme for describing the polycrystalline elasto-plastic deformation based on Eshelby's inclusion theory [117], but this scheme overestimated the effect of internal stress since only elastic interaction among grains was considered. Moreover, Hill [118] proposed a general incremental self-consistent homogenization scheme by considering the plastic interaction. However, the above-mentioned self-consistent homogenization schemes are rate-independent. Hutchinson [119] further proposed an incremental viscoplastic self-consistent homogenization scheme to simulate the creep of polycrystalline aggregates. Lebensohn and Tomé [105] extended the self-consistent homogenization scheme to solve the anisotropic viscoplastic deformation of hexagonal close-packed crystals. In the self-consistent method, each grain is regarded as an elliptical inclusion embedded in a uniform medium representing the overall response of all grains, and equilibrium conditions and compatibility should be considered. The self-consistent scheme is an effective method to investigate the deformation and texture evolution of polycrystalline materials. Therefore, many scholars have studied the plastic deformation and corresponding texture evolution of polycrystalline Mg alloys using the self-consistent homogenization scheme and considered the dislocation slipping in the twins, detwinning, solid solution strengthening, hardening caused by dislocation transformation, and other features [106–109]. The following paragraphs briefly introduce typical crystal plasticity-based constitutive models considering twinning and detwinning.

Researchers [120–123] proposed a crystal plasticity-based model that considers the twinning and detwinning of Mg alloys, which was named the twinning–detwinning (TDT) model. The TDT model in combination with an elasto–visco–plastic self-consistent homogenization scheme was used to describe the compression–tension and tension–compression–tension deformations of rolled Mg alloys. In the TDT model, the twinning and detwinning are represented by four processes: twin nucleation, growth, shrinkage, and re-twinning. The twin nucleation in the twinning system of the matrix $\left(\boldsymbol{s}^{i\mathrm{M}}, \boldsymbol{n}^{i\mathrm{M}}\right)$ is related to its RSS; that is, $\tau^{i\mathrm{M}} = \boldsymbol{s}^{i\mathrm{M}} \cdot \boldsymbol{\sigma} \cdot \boldsymbol{n}^{i\mathrm{M}}$, where $\boldsymbol{\sigma}$ is the Cauchy stress applied to the matrix, $\boldsymbol{s}^{i\mathrm{M}}$ and $\boldsymbol{n}^{i\mathrm{M}}$ are the twining plane shear and normal directions, respectively. The corresponding change in the twin volume fraction is expressed as

$$\dot{f}^i_{\mathrm{TN}} = \begin{cases} \dot{\gamma}_0 \left|\tau^{i\mathrm{M}} / \tau^{\mathrm{TN}}_{\mathrm{cr}}\right|^{1/m} / \gamma^{\mathrm{tw}}, & \tau^{i\mathrm{M}} > 0 \\ 0, & \tau^{i\mathrm{M}} \le 0 \end{cases} \tag{8}$$

where $\tau^{\mathrm{TN}}_{\mathrm{cr}}$ is the CRSS for the twin nucleation, $\dot{\gamma}_0$ is the reference shear rate, γ^{tw} is the twinning shear strain (set as 0.129), and m is the strain rate sensitivity. Twin growth occurs after the twin nucleation when the RSS on the twinning system becomes higher than the CRSS of twin growth. The CRSS of twin growth is usually lower than that of twin nucleation. To consider the stress difference between the matrix and twin, and the repartition of twin shear in the matrix and twin, the twin growth can be taken as two processes, i.e., matrix reduction and twin propagation, activated by the average stresses in the matrix and twin, respectively. The matrix reduction is realized by the twin boundary migration induced by the RSS in the matrix $\tau^{i\mathrm{M}} = \boldsymbol{s}^{i\mathrm{M}} \cdot \boldsymbol{\sigma} \cdot \boldsymbol{n}^{i\mathrm{M}}$, and the corresponding change in the twin volume fraction is

$$\dot{f}^i_{\mathrm{MR}} = \begin{cases} \dot{\gamma}_0 \left|\tau^{i\mathrm{M}} / \tau^{\mathrm{TG}}_{\mathrm{cr}}\right|^{1/m} / \gamma^{\mathrm{tw}}, & \tau^{i\mathrm{M}} > 0 \\ 0, & \tau^{i\mathrm{M}} \le 0 \end{cases} \tag{9}$$

The twin propagation is accomplished through the migration of the twin boundary toward the matrix, driven by the RSS in the twin $\tau^{i\mathrm{T}} = \boldsymbol{s}^{i\mathrm{T}} \cdot \boldsymbol{\sigma}^{i\mathrm{T}} \cdot \boldsymbol{n}^{i\mathrm{T}}$, where $\boldsymbol{s}^{i\mathrm{T}} = \boldsymbol{Q} \cdot \boldsymbol{s}^{i\mathrm{M}}$, $\boldsymbol{n}^{i\mathrm{T}} = \boldsymbol{Q} \cdot \boldsymbol{n}^{i\mathrm{M}}$ and, $\boldsymbol{Q} = 2\boldsymbol{n}^{i\mathrm{M}} \otimes \boldsymbol{n}^{i\mathrm{M}} - \boldsymbol{I}$. The change in the twin volume caused by the twin propagation can be expressed as

$$\dot{f}^i_{\mathrm{TP}} = \begin{cases} \dot{\gamma}_0 \left|\tau^{i\mathrm{T}} / \tau^{\mathrm{TG}}_{\mathrm{cr}}\right|^{1/m} / \gamma^{\mathrm{tw}}, & \tau^{i\mathrm{T}} < 0 \\ 0, & \tau^{i\mathrm{T}} \ge 0 \end{cases} \tag{10}$$

Twin shrinkage (i.e., detwinning) is the reverse operation of twin growth and thus consists of two aspects: matrix propagation and twin reduction. The corresponding changes in the twin volume fractions $\dot{f}^i_{\mathrm{MP}}$ and $\dot{f}^i_{\mathrm{TR}}$ are given by Eqs. (11) and (12), respectively.

$$\dot{f}^i_{\mathrm{MP}} = \begin{cases} -\dot{\gamma}_0 \left|\tau^{i\mathrm{M}} / \tau^{\mathrm{TS}}_{\mathrm{cr}}\right|^{1/m} / \gamma^{\mathrm{tw}}, & \tau^{i\mathrm{M}} < 0 \\ 0, & \tau^{i\mathrm{M}} \ge 0 \end{cases} \tag{11}$$

$$\dot{f}^i_{\mathrm{TR}} = \begin{cases} -\dot{\gamma}_0 \left|\tau^{i\mathrm{T}} / \tau^{\mathrm{TS}}_{\mathrm{cr}}\right|^{1/m} / \gamma^{\mathrm{tw}}, & \tau^{i\mathrm{T}} > 0 \\ 0, & \tau^{i\mathrm{T}} \le 0 \end{cases} \tag{12}$$

Finally, the evolution equation of the twin volume fraction including twin growth and shrinkage is expressed as

$$\dot{f}^i = f^{\mathrm{M}} \left(\dot{f}^i_{\mathrm{MR}} + \dot{f}^i_{\mathrm{MP}}\right) + f^i \left(\dot{f}^i_{\mathrm{TP}} + \dot{f}^i_{\mathrm{TR}}\right) \tag{13}$$

where f^{M} is the volume fraction of the matrix.

Fig. 13 shows the simulated and experimental results of rolled AZ31Mg alloy during cyclic loadings with 3% strain amplitude and in various loading directions. The anisotropic behavior and cyclic deformation characteristics of the rolled AZ31Mg alloy are reasonably simulated by the TDT model, since the model reflects the evolutions of twinning and detwinning with four processes: twin nucleation, growth, shrinkage, and re-twinning. However, empirical hardening rules are adopted to describe the interaction among dislocation slipping, twinning, and detwinning. Moreover, the model is verified only by the strain-controlled cyclic deformation. Its rationality to predict the ratchetting of Mg alloys in the stress-controlled cyclic tests, especially for the multiaxial ratchetting, should be further validated.

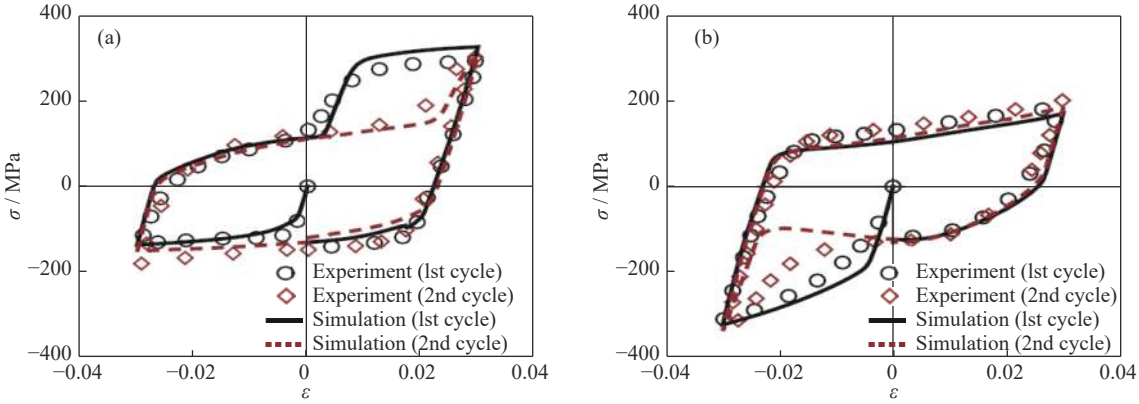

Fig. 13. Experimental and simulated stress–strain results of rolled AZ31Mg alloy in cyclic tests (applied strain amplitude is 3%): (a) compression–tension–compression along the radial direction; (b) compression–tension–compression along the ND. Reprinted from *Int. J. Plast.*, 49, H. Wang, P.D. Wu, J. Wang, and C.N. Tomé, A crystal plasticity model for hexagonal close packed (HCP) crystals including twinning and de-twinning mechanisms, 36-52, Copyright 2013, with permission from Elsevier.

3.2.2. Models based on explicit scale-transition rule

The above-mentioned self-consistent homogenization approaches can effectively establish the scale-transition relationship between single-crystal and polycrystalline aggregates, but they are very time consuming, especially for the cyclic plasticity of polycrystalline materials. Thus, other scale-transition schemes should be developed to overcome the time-consumption limitation. To achieve this aim, Cailletaud and Pilvin [124] developed an explicit scale-transition scheme (i.e., β-rule) by assuming elastic isotropy to calculate the local stress and strain tensors; through this scheme, the stress–strain response of polycrystalline aggregates is easily obtained from that of single-crystal grains. An intragranular nonlinear variable and its volume average over all the grains are introduced to reflect the local residual stress. The β-rule is widely used to simulate the cyclic plasticity of polycrystalline materials. Three typical constitutive models are briefly introduced as follows:

(1) Guillemer–Clavel–Cailletaud model.

Guillemer *et al.* [57] proposed a crystal plasticity-based constitutive model to reproduce the cyclic plasticity of extruded pure Mg by referring to relative experimental phenomena. In [57], the twinning was assumed to be related to the stress applied to the matrix and occurred when the RSS was larger than the CRSS of twinning systems and the trace of the stress tensor was negative. The twinning rate for a given variant was determined by the equivalent plastic strain caused by the dislocation slipping in the matrix:

$$\text{Twinning}: \text{if trace}\left(\boldsymbol{\sigma}^{\mathrm{g0}}\right)<0 \text{ and } \left\|\tau^{\mathrm{t}}\right\| = \boldsymbol{\sigma}^{\mathrm{g0}}:\boldsymbol{m}^{\mathrm{t}} > \tau_{\mathrm{tw}} \quad (14)$$

$$\text{Twinning rate}: \dot{\xi}^{\mathrm{gt}} = k_{\mathrm{c}}\left(\xi_{\max}-\xi^{\mathrm{g}}\right)\left(\xi_{\max}-\xi^{\mathrm{gt}}\right)\left\|\dot{\boldsymbol{\varepsilon}}^{\mathrm{g0}}\right\| \quad (15)$$

where k_{c} is a material parameter determining the twinning intensity for a given dislocation slipping; $\xi_{\max}$ is a parameter used to control the twinning rate; ξ^{g} is the total twin volume fraction in grain g; ξ^{gt} is the twin volume fraction of variant t in grain. The β-rule was adopted to transfer the stress from the macroscopic scale to the single-crystal grain scale:

$$\boldsymbol{\sigma}^{\mathrm{g}} = \boldsymbol{\sigma} + C\left(\boldsymbol{\beta}-\boldsymbol{\beta}^{\mathrm{g}}\right) \quad (16)$$

$$\dot{\boldsymbol{\beta}}^{\mathrm{g}} = \dot{\boldsymbol{\varepsilon}}^{\mathrm{g}} - D\boldsymbol{\beta}^{\mathrm{g}}\left\|\dot{\boldsymbol{\varepsilon}}^{\mathrm{g}}\right\| \quad (17)$$

To transfer the stress from the grain scale to the matrix scale:

$$\boldsymbol{\sigma}^{\mathrm{g0}} = \boldsymbol{\sigma}^{\mathrm{g}} + C_0\left(\boldsymbol{\beta}^{\mathrm{g}}-\boldsymbol{\beta}^{\mathrm{g0}}\right) \quad (18)$$

$$\dot{\boldsymbol{\beta}}^{\mathrm{g0}} = \dot{\boldsymbol{\varepsilon}}^{\mathrm{g0}} - D_0\boldsymbol{\beta}^{\mathrm{g0}}\left\|\dot{\boldsymbol{\varepsilon}}^{\mathrm{g0}}\right\| \quad (19)$$

To transfer the stress from the grain scale to the twin scale:

$$\boldsymbol{\sigma}^{\mathrm{gt}} = \boldsymbol{\sigma}^{\mathrm{g}} + C_{\mathrm{t}}\left(\boldsymbol{\beta}^{\mathrm{g}}-\boldsymbol{\beta}^{\mathrm{gt}}\right) \quad (20)$$

$$\dot{\boldsymbol{\beta}}^{\mathrm{gt}} = \dot{\boldsymbol{\varepsilon}}^{\mathrm{gt}} - D_{\mathrm{t}}\boldsymbol{\beta}^{\mathrm{gt}}\left\|\dot{\boldsymbol{\varepsilon}}^{\mathrm{gt}}\right\| \quad (21)$$

The average internal stresses of polycrystalline aggregates are defined as

$$\boldsymbol{\beta} = \sum_{g\in\mathcal{G}} f^{\mathrm{g}}\boldsymbol{\beta}^{\mathrm{g}}, \boldsymbol{\beta}^{\mathrm{g}} = \left(1-\xi^{\mathrm{g}}\right)\boldsymbol{\beta}^{\mathrm{g0}} + \sum_{t\in\mathcal{I}}\xi^{\mathrm{gt}}\boldsymbol{\beta}^{\mathrm{gt}} \quad (22)$$

where $\boldsymbol{\sigma}$ and $\boldsymbol{\varepsilon}^{\mathrm{g}}$ are the macro stress and plastic strain, respectively; $\boldsymbol{\beta}$ represents the volume average value of $\boldsymbol{\beta}^{\mathrm{g}}$ over the all grains in the polycrystalline aggregates; C and D are two material parameters of β-rule; the superscripts g, g0, and gt represent the local tensors in the grain, the matrix, and the twin, respectively.

Also, in [57], the twins formed during the cyclic deformation of Mg and its alloys were considered, and the β-rule was used in the intra- and inter-granular scales. The twinning and detwinning of polycrystalline Mg and its alloys were described by the crystal plasticity theory. The cyclic deformation of polycrystalline pure Mg under the symmetrical strain-controlled cyclic loading condition with a plastic strain amplitude of 0.4% was simulated by the proposed model, and the simulated and experimental results are given in Fig. 14. The S-shaped stress–strain curves at the first cycle and after 100 cycles could be reasonably simulated by the model; however, the model was only verified under small deformation (e.g.,

with plastic strain amplitudes of 0.1% and 0.4%). For other cyclic loading cases, the capability of the proposed model should be further verified. More importantly, the model was constructed only based on the experimental results of polycrystalline pure Mg under the strain-controlled cyclic loading conditions. The ratchetting of Mg and its alloys during the stress-controlled cyclic tests, as reviewed in Section 2.1.2, cannot be reasonably simulated by the model.

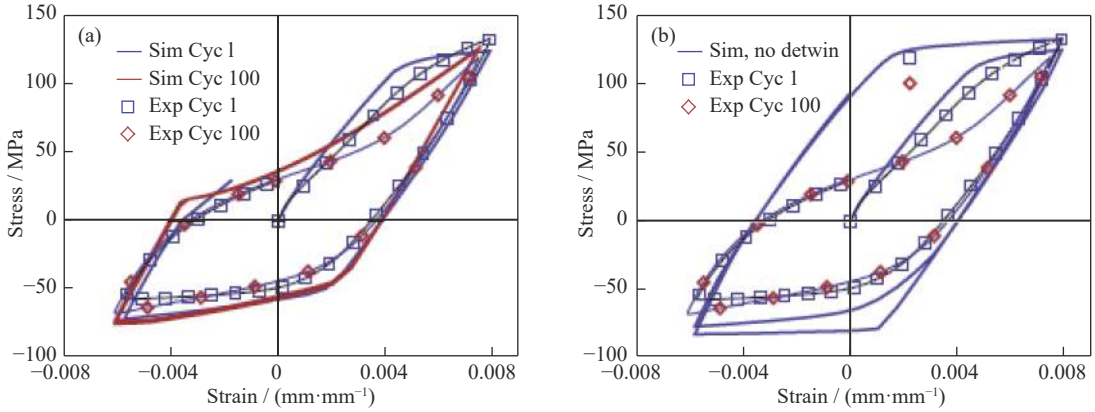

Fig. 14. Simulated and experimental stress–strain curves in the fully cyclic test with a plastic strain amplitude of 0.4%: (a) simulated by the model with detwinning; (b) simulated results by the mode without detwinning. Reprinted from *Int. J. Plast.*, 27, C. Guillemer, M. Clavel, and G. Cailletaud, Cyclic behavior of extruded magnesium: Experimental, microstructural and numerical approach, 2068-2084, Copyright 2011, with permission from Elsevier.

(2) Yu–Kang–Kan and Li–Kang–Yu models.

To describe the ratchetting of Mg and its alloys, at first, Yu *et al.* [125] introduced back stress into each slip system of single-crystal Mg and its alloys and assumed that the evolution of the back stress satisfied the classic Armstrong–Frederick kinematic hardening rule [126]; that is

$$\dot{x}^{i\beta} = c\dot{\gamma}^{i\beta}_{\text{slip}} - bx^{i\beta}\left|\dot{\gamma}^{i\beta}_{\text{slip}}\right| \tag{23}$$

where c and b are two material parameters; $\dot{\gamma}^{i\beta}_{\text{slip}}$ is the rate of dislocation slipping. Meanwhile, a linear isotropic hardening rule was used to reflect the strain hardening caused by dislocation slipping; that is,

$$\dot{\tau}^{i\beta}_{\text{c}} = \sum_{i=1}^{\text{nslip}} H_{ij}\left|\dot{\gamma}^{i\beta}_{\text{slip}}\right| \tag{24}$$

$$H_{ij} = h\left[q + (1-q)\delta_{ij}\right] \tag{25}$$

where H_{ij} is the hardening coefficient matrix reflecting self- and latent-hardening; h is the hardening modulus (the basal, prismatic, and pyramidal slips correspond to different hardening moduli); q is a material parameter controlling the latent-hardening extent; δ_{ij} is Kornecker function.

Finally, the β-rule was adopted to obtain the polycrystalline response from that of single-crystal grain. In [125], the Yu–Kang–Kan model could reasonably describe the ratchetting of rolled polycrystalline AZ91 Mg alloy with different stress amplitudes and mean stresses, while the plastic deformation was dominated only by the dislocation slipping. Although the Yu–Kang–Kan model could simulate the ratchetting of rolled AZ91 Mg alloy, only the dislocation slipping was addressed. Thus, the complicated cyclic plastic deformation of Mg and its alloys involving the dislocation slipping, twinning, and detwinning, as well as their interactions (as reviewed in Section 2.1.2), cannot be predicted by the Yu–Kang–Kan model.

To more reasonably predict the ratchetting of Mg alloys, based on the Yu–Kang–Kan model [125], Li *et al.* [127] considered dislocation slipping, twinning, and detwinning, as well as their interactions by proposing new kinematic and isotropic hardening rules. Then, they established a new crystal plasticity-based constitutive model, called the Li–Kang–Yu model. This model adopts pseudo-linear kinematic hardening rules to describe the twinning and detwinning:

$$\dot{x}^{i}_{\text{twin}} = k_{\text{twin}}\dot{\gamma}^{i}_{\text{twin}} = \{k_{0,\text{twin}} + \underbrace{k_{\text{sat,twin}}[1-(\exp - b_1\gamma^{i}_{\text{c,detwin}})]}_{\substack{\text{Kinematic hardenning modulus}\\ \text{assiociated with detwinning}}}\}\dot{\gamma}^{i}_{\text{twin}} \tag{26}$$

$$\dot{x}^{i}_{\text{detwin}} = k_{\text{detwin}}\dot{\gamma}^{i}_{\text{twin}} = \{k_{0,\text{detwin}} + \underbrace{k_{\text{sat,detwin}}[1-\exp(-b_2\gamma^{i}_{\text{c,detwin}})]}_{\substack{\text{Kinematic hardenning modulus}\\ \text{assiociated with detwinning}}} + \underbrace{k'_{\text{sat,detwin}}[1-\exp(-b_3\gamma^{i}_{\text{c,twin}})]}_{\substack{\text{Kinematic hardenning modulus}\\ \text{assiociated with twinning}}}\}\dot{\gamma}^{i}_{\text{twin}} \tag{27}$$

where $k_{0,\text{twin}}$, $k_{\text{sat,twin}}$, $k_{0,\text{detwin}}$, $k_{\text{sat,detwin}}$, and $k'_{\text{sat,detwin}}$ are parameters related to the hardening moduli; b_1, b_2 and b_3 are the parameters characterize the hardening rate. The kinematic hardening moduli evolve with the accumulated plastic deformation resulting from the twinning/detwinning, reflecting

the evolutions of the back stresses corresponding to the twinning/detwinning during the cyclic deformation.

The β-rule was also employed here to obtain the overall response of polycrystalline Mg alloys. As shown in Fig. 15, the Li–Kang–Yu model can reasonably describe the uniaxial ratchetting of extruded AZ31 Mg alloy with various mean stresses and stress amplitudes and at room temperature. However, the isotropic and kinematic hardening rules adopted in the model for the twinning and detwinning are based on the macroscopic observation; no physical mechanisms of twinning and detwinning are directly involved, which should be further improved. Moreover, the Li–Kang–Yu model predicts only the uniaxial ratchetting at room temperature; the ratchetting of Mg alloys at high temperatures and under multiaxial cyclic loading conditions has not been addressed yet; it should be considered in the future.

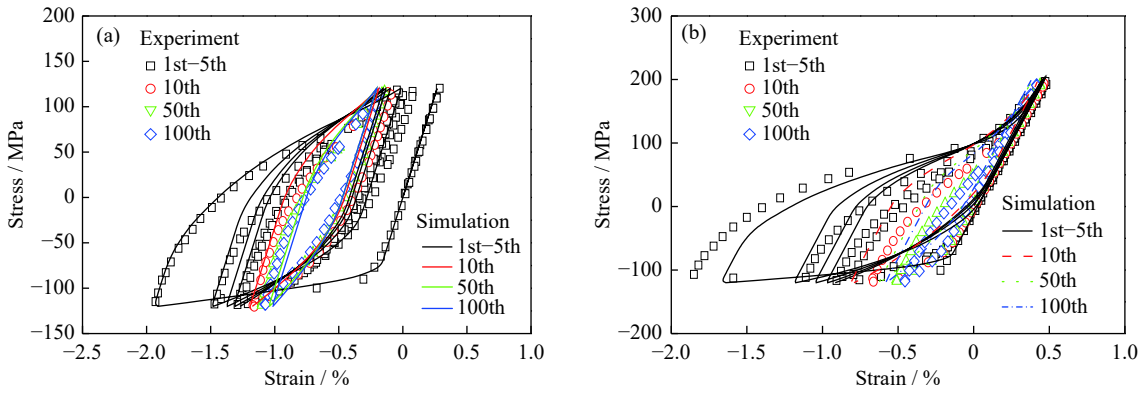

Fig. 15. Experimental and simulated stress–strain curves of extruded AZ31 Mg alloy with different stress levels: (a) for (0 ± 120) MPa; (b) for (40 ± 160) MPa. Reprinted from *Int. J. Mech. Sci.*, 179, H. Li, G.Z. Kang, and C. Yu, Modeling uniaxial ratchetting of magnesium alloys by a new crystal plasticity considering dislocation slipping, twinning and detwinning mechanisms, 105660, Copyright 2020, with permission from Elsevier.

In summary, the dislocation slipping and twinning/detwinning that occur in the cyclic plasticity of Mg alloys and their interactions can be described by the developed crystal plasticity-based constitutive models; however, these models must be constructed based on some assumptions and simplifications because of the complexity of the interactions among multiple plastic deformation mechanisms; moreover, some important microstructure features (such as grain boundaries, precipitates, texture and dynamic recrystallization) and their interactions with dislocation slipping and twinning/detwinning have not been addressed yet. Therefore, it is still a big challenge to model the cyclic plasticity of Mg alloys by reasonably considering related physical mechanisms. Much more effort is needed to enhance the reasonability and prediction capability of crystal plasticity-based cyclic constitutive models.

4. Summary and recommendation

This study shows that positive progress has been achieved in the experimental and theoretical research on the cyclic plasticity of Mg alloys, and a solid foundation has been provided for the further development and application of the alloys. The conclusions can be summarized as follows:

(1) In strain-controlled cyclic conditions, wrought Mg alloys exhibit tension–compression asymmetry, including asymmetrical S-shaped stress–strain hysteresis loop, due to the activation of dislocation slipping and/or twinning/detwinning at different loading stages. Cyclic hardening occurs and is affected by various loading factors, including applied strain amplitude, strain rate, loading path, and test temperature. However, the stress–strain hysteresis loops of cast Mg alloys are almost symmetrical due to the absence of an obvious texture, although asymmetric tension–compression yielding stresses have been observed in some studies.

(2) In stress-controlled cyclic tests, remarkable ratchetting occurs in wrought Mg alloys and depends strongly on the stress levels and multiaxial loading paths (proportional and non-proportional paths). The stress level determines the plastic deformation mechanism activated during the ratchetting and then results in different shapes of stress–strain hysteresis loops and varied rate and temperature dependences of ratchetting.

(3) Significant interaction between the dislocation slipping and twinning occurs during the cyclic plastic deformation of Mg alloys; that is, the twin boundary is a significant hindrance to the dislocation slipping, and the dislocations accumulated at the twin boundary can reduce the twinning activity. In addition, the occurrence of twin–twin boundaries restrains subsequent twinning/detwinning. Finally, complex interactions among various plastic deformation mechanisms occur during the cyclic plastic deformation of Mg alloys and are affected by many factors, such as grain orientation, intragranular distribution of twins, and volume fraction of twins.

(4) Existing phenomenological constitutive models can capture the tension–compression asymmetry and plastic anisotropy of wrought Mg alloys and can reproduce the cyclic plastic deformation under some specific loading conditions.

(5) The proposed crystal plasticity-based constitutive models consider different plastic deformation mechanisms of Mg alloys, as well as the texture evolution. The proposed models can reasonably reproduce the cyclic plasticity of Mg alloys in some specific cases (including uniaxial ratchetting at room temperature).

However, the interactions and evolutions of complicated microstructures involved in the cyclic plasticity of Mg alloys under complex loading conditions (e.g., multiaxial loading conditions and/or elevated temperatures) have not been clearly realized, and the current established constitutive models (either phenomenological or crystal plasticity-based models) cannot describe the cyclic plasticity of Mg alloys under complex cyclic loading conditions. This implies that many topics require further investigation. Thus, the following issues should be addressed in the future:

(1) The macroscopic experimental investigations on the cyclic plasticity of Mg alloys should be strengthened, since experimental data reflecting the multiaxial cyclic plasticity at elevated temperatures and with various loading histories and loading rates are still rare.

(2) Much more microscopic experimental observations are necessary to clarify the interactions of various plastic deformation mechanisms in Mg alloys, especially for the evolutions of dislocation and twins at different stages of cyclic deformation. The interactions of dislocations and twins with other microstructures, such as grain boundary, precipitates, texture, and recrystallization are also important issues to capture the physical nature of cyclic plasticity in Mg alloys.

(3) Molecular dynamics, discrete dislocation dynamics, and phase-field simulations are useful supplements to reveal the physical nature of cyclic plasticity in Mg and its alloys, especially for the polycrystalline ones.

(4) The macroscopic phenomenological constitutive model of Mg alloys should be further developed by considering the multiaxial cyclic plasticity and its corresponding rate and temperature dependences. Also, the influence of loading history on the cyclic plasticity of Mg alloys should be reasonably considered.

(5) Crystal plasticity-based constitutive models of Mg alloys should be further improved to capture the complicated plastic deformation mechanisms and their interactions more physically and comprehensively. Interactions between basic plastic deformation mechanisms and other microstructures (grain boundary, precipitates, secondary phase, texture, and recrystallization) should be further addressed.

(6) An efficient and robust integration algorithm should be developed to implement the developed constitutive models into a finite element code, which is important for structural analysis, since high nonlinearity is always encountered in the constitutive models of Mg alloys.

(7) The multi-physical-field coupled cyclic plasticity of Mg alloys is also a big challenge, since thermo-mechanical and thermo–chemo-mechanical coupled issues are often encountered in the practical applications of Mg alloys in the ambient media with high corrosion and varying temperatures.

Acknowledgements

This work was financially supported by the National Natural Science Foundation of China (No. 11532010) and Doctoral Innovation Fund Program of Southwest Jiaotong University.

References

[1] E. Aghion, B. Bronfin, and D. Eliezer, The role of the magnesium industry in protecting the environment, *J. Mater. Process. Technol.*, 117(2001), No. 3, p. 381.

[2] D. Eliezer, E. Aghion, and F.H. (Sam) Froes, Magnesium science, technology and applications, *Adv. Perform. Mater.*, 5(1998), No. 3, p. 201.

[3] B.L. Mordike and T. Ebert, Magnesium: Properties—applications—potential, *Mater. Sci. Eng. A*, 302(2001), No. 1, p. 37.

[4] T.M. Pollock, Weight loss with magnesium alloys, *Science*, 328(2010), No. 5981, p. 986.

[5] E.A. Ball and P.B. Prangnell, Tensile-compressive yield assymetries in high strength wrought magnesium alloys, *Scr. Metall. Mater.*, 31(1994), No. 2, p. 111.

[6] M.R. Barnett, Z. Keshavarz, A.G. Beer, and D. Atwell, Influence of grain size on the compressive deformation of wrought Mg–3Al–1Zn, *Acta Mater.*, 52(2004), No. 17, p. 5093.

[7] X.Y. Lou, M. Li, R.K. Boger, S.R. Agnew, and R.H. Wagoner, Hardening evolution of AZ31B Mg sheet, *Int. J. Plast.*, 23(2007), No. 1, p. 44.

[8] J.P. Nobre, U. Noster, M. Kornmeier, A.M. Dias, and B. Scholtes, Deformation asymmetry of AZ31 wrought magnesium alloy, *Key Eng. Mater.*, 230-232(2002), p. 267.

[9] Y. Xiong, Q. Yu, and Y.Y. Jiang, An experimental study of cyclic plastic deformation of extruded ZK60 magnesium alloy under uniaxial loading at room temperature, *Int. J. Plast.*, 53(2014), p. 107.

[10] H. Li, G.Z. Kang, C. Yu, and Y.J. Liu, Experimental investigation on temperature-dependent uniaxial ratchetting of AZ31B magnesium alloy, *Int. J. Fatigue*, 120(2019), p. 33.

[11] A. Gryguc, S.K. Shaha, S.B. Behravesh, H. Jahed, M. Wells, B. Williams, and X. Su, Monotonic and cyclic behaviour of cast and cast-forged AZ80 Mg, *Int. J. Fatigue*, 104(2017), p. 136.

[12] J. Albinmousa, H. Jahed, and S. Lambert, Cyclic behaviour of wrought magnesium alloy under multiaxial load, *Int. J. Fatigue*, 33(2011), No. 8, p. 1127.

[13] J. Albinmousa, H. Jahed, and S. Lambert, Cyclic axial and cyclic torsional behaviour of extruded AZ31B magnesium alloy, *Int. J. Fatigue*, 33(2011), No. 11, p. 1403.

[14] S. Begum, D.L. Chen, S. Xu, and A.A. Luo, Strain-controlled

low-cycle fatigue properties of a newly developed extruded magnesium alloy, *Metall. Mater. Trans. A*, 39(2008), No. 12, p. 3014.

[15] C. Chen, T.M. Liu, C.L. Lv, L.W. Lu, and D.Z. Luo, Study on cyclic deformation behavior of extruded Mg–3Al–1Zn alloy, *Mater. Sci. Eng. A*, 539(2012), p. 223.

[16] L.J. Chen, C.Y. Wang, W. Wu, Z. Liu, G.M. Stoica, L. Wu, and P.K. Liaw, Low-cycle fatigue behavior of an as-extruded AM50 magnesium alloy, *Metall. Mater. Trans. A*, 38(2007), No. 13, p. 2235.

[17] T. Hama, Y. Kariyazaki, N. Hosokawa, H. Fujimoto, and H. Takuda, Work-hardening behaviors of magnesium alloy sheet during in-plane cyclic loading, *Mater. Sci. Eng. A*, 551(2012), p. 209.

[18] S. Dong, Q. Yu, Y.Y. Jiang, J. Dong, F.H. Wang, L. Jin, and W.J. Ding, Characteristic cyclic plastic deformation in ZK60 magnesium alloy, *Int. J. Plast.*, 91(2017), p. 25.

[19] Y. Xiong, Q. Yu, and Y.Y. Jiang, Cyclic deformation and fatigue of extruded AZ31B magnesium alloy under different strain ratios, *Mater. Sci. Eng. A*, 649(2016), p. 93.

[20] A.H. Pahlevanpour, S.M.H. Karparvarfard, S.K. Shaha, S.B. Behravesh, S. Adibnazari, and H. Jahed, Anisotropy in the quasi-static and cyclic behavior of ZK60 extrusion: Characterization and fatigue modeling, *Mater. Des.*, 160(2018), p. 936.

[21] C. Wang, T.J. Luo, J.X. Zhou, and Y.S. Yang, Anisotropic cyclic deformation behavior of extruded ZA81M magnesium alloy, *Int. J. Fatigue*, 96(2017), p. 178.

[22] S.M.H. Karparvarfard, S.K. Shaha, S.B. Behravesh, H. Jahed, and B.W. Williams, Fatigue characteristics and modeling of cast and cast-forged ZK60 magnesium alloy, *Int. J. Fatigue*, 118(2019), p. 282.

[23] S.M.A.K. Mohammed, D.J. Li, X.Q. Zeng, and D.L. Chen, Cyclic deformation behavior of a high zinc-containing cast magnesium alloy, *Int. J. Fatigue*, 125(2019), p. 1.

[24] K. Máthis, P. Beran, J. Čapek, and P. Lukáš, *In-situ* neutron diffraction and acoustic emission investigation of twinning activity in magnesium, *J. Phys. Conf. Ser.*, 340(2012), art. No. 12096.

[25] S.H. Park, J.H. Lee, B.G. Moon, and B.S. You, Tension–compression yield asymmetry in as-cast magnesium alloy, *J. Alloys Compd.*, 617(2014), p. 277.

[26] S. Begum, D.L. Chen, S. Xu, and A.A. Luo, Effect of strain ratio and strain rate on low cycle fatigue behavior of AZ31 wrought magnesium alloy, *Mater. Sci. Eng. A*, 517(2009), No. 1-2, p. 334.

[27] C. Wang, T.J. Luo, and Y.S. Yang, Low cycle fatigue behavior of the extruded AZ80 magnesium alloy under different strain amplitudes and strain rates, *J. Magnesium Alloys*, 4(2016), No. 3, p. 181.

[28] G. Chen, J.W. Gao, Y. Cui, H. Gao, X. Guo, and S.Z. Wu, Effects of strain rate on the low cycle fatigue behavior of AZ31B magnesium alloy processed by SMAT, *J. Alloys Compd.*, 735(2018), p. 536.

[29] J.H. Kim, D. Kim, Y.S. Lee, M.G. Lee, K. Chung, H.Y. Kim, and R.H. Wagoner, A temperature-dependent elasto-plastic constitutive model for magnesium alloy AZ31 sheets, *Int. J. Plast.*, 50(2013), p. 66.

[30] K. Piao, J.K. Lee, J.H. Kim, H.Y. Kim, K. Chung, F. Barlat, and R.H. Wagoner, A sheet tension/compression test for elevated temperature, *Int. J. Plast.*, 38(2012), p. 27.

[31] L. Jiang, J.J. Jonas, R.K. Mishra, A.A. Luo, A.K. Sachdev, and S. Godet, Twinning and texture development in two Mg alloys subjected to loading along three different strain paths, *Acta Mater.*, 55(2007), No. 11, p. 3899.

[32] F.H. Wang, M.L. Feng, Y.Y. Jiang, J. Dong, and Z.Y. Zhang, Cyclic shear deformation and fatigue of extruded Mg–Gd–Y magnesium alloy, *J. Mater. Sci. Technol.*, 39(2020), p. 74.

[33] J.X. Zhang, Q. Yu, Y.Y. Jiang, and Q.Z. Li, An experimental study of cyclic deformation of extruded AZ61A magnesium alloy, *Int. J. Plast.*, 27(2011), No. 5, p. 768.

[34] Q. Yu, J.X. Zhang, Y.Y. Jiang, and Q.Z. Li, Multiaxial fatigue of extruded AZ61A magnesium alloy, *Int. J. Fatigue*, 33(2011), No. 3, p. 437.

[35] H. Li, G.Z. Kang, Y.J Liu, and H. Jiang, Non-proportionally multiaxial cyclic deformation of AZ31 magnesium alloy: Experimental observations, *Mater. Sci. Eng. A*, 671(2016), p. 70.

[36] A.A. Roostaei and H. Jahed, Multiaxial cyclic behaviour and fatigue modelling of AM30 Mg alloy extrusion, *Int. J. Fatigue*, 97(2017), p. 150.

[37] A. Gryguć, S.B. Behravesh, S.K. Shaha, H. Jahed, M. Wells, B. Williams, and X. Su, Multiaxial cyclic behaviour of extruded and forged AZ80 Mg alloy, *Int. J. Fatigue*, 127(2019), p. 324.

[38] J.L. Chaboche, A review of some plasticity and viscoplasticity constitutive theories, *Int. J. Plast.*, 24(2008), No. 10, p. 1642.

[39] G.Z. Kang, Ratchetting: Recent progresses in phenomenon observation, constitutive modeling and application, *Int. J. Fatigue*, 30(2008), No. 8, p. 1448.

[40] O. Nobutada, Recent topics in constitutive modeling of cyclic plasticity and viscoplasticity, *Appl. Mech. Rev.*, 43(1990), No. 11, p. 283.

[41] G.Z. Kang, Y. Chao, Y.J. Liu, and G.F. Quan, Uniaxial ratchetting of extruded AZ31 magnesium alloy: Effect of mean stress, *Mater. Sci. Eng. A*, 607(2014), p. 318.

[42] Z.F. Yan, D.H. Wang, X.L. He, W.X. Wang, H.X. Zhang, P. Dong, C.H. Li, Y.L. Li, J. Zhou, Z. Liu, and L.Y. Sun, Deformation behaviors and cyclic strength assessment of AZ31B magnesium alloy based on steady ratcheting effect, *Mater. Sci. Eng. A*, 723(2018), p. 212.

[43] Y.C. Lin, Z.H. Liu, X.M. Chen, and J. Chen, Uniaxial ratcheting and fatigue failure behaviors of hot-rolled AZ31B magnesium alloy under asymmetrical cyclic stress-controlled loadings, *Mater. Sci. Eng. A*, 573(2013), p. 234.

[44] Y.C. Lin, X.M. Chen, and G. Chen, Uniaxial ratcheting and low-cycle fatigue failure behaviors of AZ91D magnesium alloy under cyclic tension deformation, *J. Alloys Compd.*, 509(2011), No. 24, p. 6838.

[45] L. Meng, S. Hallais, A. Tanguy, W.F. Chen, and M.L. Feng, The effect of stress rate on ratchetting behavior of rolled AZ31B magnesium alloy at 393 K and room temperature, *Mater. Res. Express*, 6(2019), No. 8, art. No. 086510.

[46] U. Noster and B. Scholtes, Cyclic deformation behavior of magnesium alloys AZ31 and AZ91 in the temperature range 20–300°C, *Mater. Sci. Forum.*, 419-422(2003), p. 103.

[47] F. Castro and Y.Y. Jiang, Fatigue of extruded AZ31B magnesium alloy under stress- and strain-controlled conditions including step loading, *Mech. Mater.*, 108(2017), p. 77.

[48] M.H. Yoo, Slip, twinning, and fracture in hexagonal close-packed metals, *Metall. Trans. A*, 12(1981), No. 3, p. 409.
[49] A. Couret and D. Caillard, An *in situ* study of prismatic glide in magnesium—I. The rate controlling mechanism, *Acta Metall.*, 33(1985), No. 8, p. 1447.
[50] R.E. Reed-Hill and W.D. Robertson, Deformation of magnesium single crystals by nonbasal slip, *JOM*, 9(1957), No. 4, p. 496.
[51] P.J.F. Stohr and J.P. Poirier, Etude en microscopie electronique du glissement pyramidal $\{11\bar{2}2\}\langle 11\bar{2}3\rangle$ dans le magnesium, *Philos. Mag.*, 25(1972), No. 6, p. 1313.
[52] T. Obara, H. Yoshinga, and S. Morozumi, $\{11\bar{2}2\}\langle 11\bar{2}3\rangle$ Slip system in magnesium, *Acta Metall.*, 21(1973), No. 7, p. 845.
[53] S. Ando, M. Tanaka, and H. Tonda, Pyramidal slip in magnesium alloy single crystals, *Mater. Sci. Forum.*, 419-422(2003), p. 87.
[54] E. Lilleodden, Microcompression study of Mg (0001) single crystal, *Scripta Mater.*, 62(2010), No. 8, p. 532.
[55] C.M. Byer, B. Li, B.Y. Cao, and K.T. Ramesh, Microcompression of single-crystal magnesium, *Scripta Mater.*, 62(2010), No. 8, p. 536.
[56] K.Y. Xie, Z. Alam, A. Caffee, and K.J. Hemker, Pyramidal I slip in *c*-axis compressed Mg single crystals, *Scripta Mater.*, 112(2016), p. 75.
[57] C. Guillemer, M. Clavel, and G. Cailletaud, Cyclic behavior of extruded magnesium: Experimental, microstructural and numerical approach, *Int. J. Plast.*, 27(2011), No. 12, p. 2068.
[58] W. Wu, Y.F. Gao, N. Li, C.M. Parish, W.J. Liu, P.K. Liaw, and K. An, Intragranular twinning, detwinning, and twinning-like lattice reorientation in magnesium alloys, *Acta Mater.*, 121(2016), p. 15.
[59] L. Lu, B.X. Bie, Q.H. Li, T. Sun, K. Fezzaa, X.L. Gong, and S.N. Luo, Multiscale measurements on temperature-dependent deformation of a textured magnesium alloy with synchrotron x-ray imaging and diffraction, *Acta Mater.*, 132(2017), p. 389.
[60] L. Lu, J.W. Huang, D. Fan, B.X. Bie, T. Sun, K. Fezzaa, X.L. Gong, and S.N. Luo, Anisotropic deformation of extruded magnesium alloy AZ31 under uniaxial compression: A study with simultaneous in situ synchrotron x-ray imaging and diffraction, *Acta Mater.*, 120(2016), p. 86.
[61] S. Dong, Q. Yu, Y.Y. Jiang, J. Dong, F.H. Wang, and W.J. Ding, Electron backscatter diffraction observations of twinning–detwinning evolution in a magnesium alloy subjected to large strain amplitude cyclic loading, *Mater. Des.*, 65(2015), p. 762.
[62] S.M. Yin, F. Yang, X.M. Yang, S.D. Wu, S.X. Li, and G.Y. Li, The role of twinning–detwinning on fatigue fracture morphology of Mg–3%Al–1%Zn alloy, *Mater. Sci. Eng. A*, 494(2008), No. 1-2, p. 397.
[63] Q. Yu, J. Wang, Y.Y. Jiang, R.J. McCabe, N. Li, and C.N. Tomé, Twin–twin interactions in magnesium, *Acta Mater.*, 77(2014), p. 28.
[64] Q. Sun, T. Xia, L. Tan, J. Tu, M. Zhang, M.H. Zhu, and X.Y. Zhang, Influence of $\{10\bar{1}2\}$ twin characteristics on detwinning in Mg–3Al–1Zn alloy, *Mater. Sci. Eng. A*, 735(2018), p. 243.
[65] L. Wu, S.R. Agnew, D.W. Brown, G.M. Stoica, B. Clausen, A. Jain, D.E. Fielden, and P.K. Liaw, Internal stress relaxation and load redistribution during the twinning–detwinning-dominated cyclic deformation of a wrought magnesium alloy, ZK60A, *Acta Mater.*, 56(2008), No. 14, p. 3699.
[66] D. Sarker, J. Friedman, and D.L. Chen, Influence of pre-strain on de-twinning activity in an extruded AM30 magnesium alloy, *Mater. Sci. Eng. A*, 605(2014), p. 73.
[67] B.M. Morrow, R.J. McCabe, E.K. Cerreta, and C.N. Tomé, *In-situ* TEM observation of twinning and detwinning during cyclic loading in Mg, *Metall. Mater. Trans. A*, 45(2013), No. 1, p. 36.
[68] L.C. Lv, Y.C. Xin, H.H. Yu, R. Hong, and Q. Liu, The role of dislocations in strain hardening of an extension twinning predominant deformation, *Mater. Sci. Eng. A*, 636(2015), p. 389.
[69] Q. Ma, H. El Kadiri, A.L. Oppedal, J.C. Baird, B. Li, M.F. Horstemeyer, and S.C. Vogel, Twinning effects in a rod-textured AM30 Magnesium alloy, *Int. J. Plast.*, 29(2012), p. 60.
[70] S. Dong, Y.Y. Jiang, J. Dong, F.H. Wang, and W.J. Ding, Cyclic deformation and fatigue of extruded ZK60 magnesium alloy with aging effects, *Mater. Sci. Eng. A*, 615(2014), p. 262.
[71] P. Chen, B. Li, D. Culbertson, and Y.Y. Jiang, Negligible effect of twin-slip interaction on hardening in deformation of a Mg–3Al–1Zn alloy, *Mater. Sci. Eng. A*, 729(2018), p. 285.
[72] H.H. Yu, Y.C. Xin, Y. Cheng, B. Guan, M.Y. Wang, and Q. Liu, The different hardening effects of tension twins on basal slip and prismatic slip in Mg alloys, *Mater. Sci. Eng. A*, 700(2017), p. 695.
[73] J. Jeong, M. Alfreider, R. Konetschnik, D. Kiener, and S.H. Oh, *In-situ* TEM observation of $\{10\bar{1}2\}$ twin-dominated deformation of Mg pillars: Twinning mechanism, size effects and rate dependency, *Acta Mater.*, 158(2018), p. 407.
[74] M.H. Yoo, Interaction of slip dislocations with twins in hcp metals, *Trans. Metall. Soc. AIME*, 245(1969), p. 2051.
[75] F.L. Wang and S.R. Agnew, Dislocation transmutation by tension twinning in magnesium alloy AZ31, *Int. J. Plast.*, 81(2016), p. 63.
[76] F.L. Wang, C.D. Barrett, R.J. McCabe, H. El Kadiri, L. Capolungo, and S.R. Agnew, Dislocation induced twin growth and formation of basal stacking faults in $\{10\bar{1}2\}$ twins in pure Mg, *Acta Mater.*, 165(2019), p. 471.
[77] F. Wang, K. Hazeli, K.D. Molodov, C.D. Barrett, T. Al-Samman, D.A. Molodov, A. Kontsos, K.T. Ramesh, H. El Kadiri, and S.R. Agnew, Characteristic dislocation substructure in $\{10\bar{1}2\}$ twins in hexagonal metals, *Scripta Mater.*, 143(2018), p. 81.
[78] Y. Chino, K. Kimura, and M. Mabuchi, Twinning behavior and deformation mechanisms of extruded AZ31 Mg alloy, *Mater. Sci. Eng. A*, 486(2008), No. 1-2, p. 481.
[79] C.F. Gu, L.S. Toth, and M. Hoffman, Twinning effects in a polycrystalline magnesium alloy under cyclic deformation, *Acta Mater.*, 62(2014), p. 212.
[80] F. Kabirian, A.S. Khan, and T. Gnäupel-Herlod, Visco-plastic modeling of mechanical responses and texture evolution in extruded AZ31 magnesium alloy for various loading conditions, *Int. J. Plast.*, 68(2015), p. 1.
[81] K.D. Molodov, T. Al-Samman, and D.A. Molodov, Profuse slip transmission across twin boundaries in magnesium, *Acta Mater.*, 124(2017), p. 397.
[82] D.F. Shi, T.M. Liu, T.Y. Wang, D.W. Hou, S.Q. Zhao, and S. Hussain, $\{10\bar{1}2\}$ Twins across twin boundaries traced by *in situ* EBSD, *J. Alloys Compd.*, 690(2017), p. 699.

[83] M. Zecevic, I.J. Beyerlein, and M. Knezevic, Activity of pyramidal I and II <c+a> slip in Mg alloys as revealed by texture development, *J. Mech. Phys. Solids*, 111(2018), p. 290.
[84] N.T. Nguyen, M.G. Lee, J.H. Kim, and H.Y. Kim, A practical constitutive model for AZ31B Mg alloy sheets with unusual stress–strain response, *Finite. Elem. Anal. Des.*, 76(2013), p. 39.
[85] C.A. Lee, M.G. Lee, O.S. Seo, N.T. Nguyen, J.H. Kim, and H.Y. Kim, Cyclic behavior of AZ31B Mg: Experiments and non-isothermal forming simulations, *Int. J. Plast.*, 75(2015), p. 39.
[86] A.A. Roostaei and H. Jahed, A cyclic small-strain plasticity model for wrought Mg alloys under multiaxial loading: Numerical implementation and validation, *Int. J. Mech. Sci.*, 145(2018), p. 318.
[87] M. Li, X.Y. Lou, J.H. Kim, and R.H. Wagoner, An efficient constitutive model for room-temperature, low-rate plasticity of annealed Mg AZ31B sheet, *Int. J. Plast.*, 26(2010), No. 6, p. 820.
[88] O. Cazacu and F. Barlat, A criterion for description of anisotropy and yield differential effects in pressure-insensitive metals, *Int. J. Plast.*, 20(2004), No. 11, p. 2027.
[89] O. Cazacu, B. Plunkett, and F. Barlat, Orthotropic yield criterion for hexagonal closed packed metals, *Int. J. Plast.*, 22(2006), No. 7, p. 1171.
[90] B. Plunkett, R.A. Lebensohn, O. Cazacu, and F. Barlat, Anisotropic yield function of hexagonal materials taking into account texture development and anisotropic hardening, *Acta Mater.*, 54(2006), No. 16, p. 4159.
[91] B. Plunkett, O. Cazacu, and F. Barlat, Orthotropic yield criteria for description of the anisotropy in tension and compression of sheet metals, *Int. J. Plast.*, 24(2008), No. 5, p. 847.
[92] J.W. Yoon, Y.S. Lou, J. Yoon, and M.V. Glazoff, Asymmetric yield function based on the stress invariants for pressure sensitive metals, *Int. J. Plast.*, 56(2014), p. 184.
[93] D.G. Tari, M.J. Worswick, U. Ali, and M.A. Gharghouri, Mechanical response of AZ31B magnesium alloy: Experimental characterization and material modeling considering proportional loading at room temperature, *Int. J. Plast.*, 55(2014), p. 247.
[94] W. Muhammad, M. Mohammadi, J.D. Kang, R.K. Mishra, and K. Inal, An elasto-plastic constitutive model for evolving asymmetric/anisotropic hardening behavior of AZ31B and ZEK100 magnesium alloy sheets considering monotonic and reverse loading paths, *Int. J. Plast.*, 70(2015), p. 30.
[95] M.G. Lee, R.H. Wagoner, J.K. Lee, K. Chung, and H.Y. Kim, Constitutive modeling for anisotropic/asymmetric hardening behavior of magnesium alloy sheets, *Int. J. Plast.*, 24(2008), No. 4, p. 545.
[96] M.G. Lee, S.J. Kim, R.H. Wagoner, K. Chung, and H.Y. Kim, Constitutive modeling for anisotropic/asymmetric hardening behavior of magnesium alloy sheets: Application to sheet springback, *Int. J. Plast.*, 25(2009), No. 1, p. 70.
[97] F. Barlat, J.J. Gracio, M.G. Lee, E.F. Rauch, and G. Vincze, An alternative to kinematic hardening in classical plasticity, *Int. J. Plast.*, 27(2011), No. 9, p. 1309.
[98] J. Lee, S.J. Kim, Y.S. Lee, J.Y. Lee, D. Kim, and M.G. Lee, Distortional hardening concept for modeling anisotropic/asymmetric plastic behavior of AZ31B magnesium alloy sheets, *Int. J. Plast.*, 94(2017), p. 74.
[99] W.J. He, T. Lin, and Q. Liu, Experiments and constitutive modeling of deformation behavior of a magnesium sheet during two-step loading, *Int. J. Solids Struct.*, 147(2018), p. 52.
[100] G.I. Taylor, Plastic Strain in Metals, *J. Jpn. Inst. Met.*, 62(1938), p. 307.
[101] E. Kröner, Zur plastischen verformung des vielkristalls, *Acta Metall.*, 9(1961), No. 2, p. 155.
[102] B. Budiansky and T.T. Wu, Theoretical prediction of plastic strains of polycrystals, [in] *Proceedings of the 4th US National Congress of Applied Mechanics*, California, 1962, p. 1175.
[103] P. Van Houtte, Simulation of the rolling and shear texture of brass by the Taylor theory adapted for mechanical twinning, *Acta Metall.*, 26(1978), No. 4, p. 591.
[104] C.N. Tomé, R.A. Lebensohn, and U.F. Kocks, A model for texture development dominated by deformation twinning: Application to zirconium alloys, *Acta Metall. Mater.*, 39(1991), No. 11, p. 2667.
[105] R.A. Lebensohn and C.N. Tome, A self-consistent anisotropic approach for the simulation of plastic deformation and texture development of polycrystals: Application to zirconium alloys, *Acta Metall. Mater.*, 41(1993), No. 9, p. 2611.
[106] S.R. Agnew, M.H. Yoo, and C.N. Tomé, Application of texture simulation to understanding mechanical behavior of Mg and solid solution alloys containing Li or Y, *Acta Mater.*, 49(2001), No. 20, p. 4277.
[107] S.H. Choi, E.J. Shin, and B.S. Seong, Simulation of deformation twins and deformation texture in an AZ31 Mg alloy under uniaxial compression, *Acta Mater.*, 55(2007), No. 12, p. 4181.
[108] S.R. Kalidindi, Incorporation of deformation twinning in crystal plasticity models, *J. Mech. Phys. Solids*, 46(1998), No. 2, p. 267.
[109] A. Staroselsky and L. Anand, A constitutive model for hcp materials deforming by slip and twinning: application to magnesium alloy AZ31B, *Int. J. Plast.*, 19(2003), No. 10, p. 1843.
[110] H. Abdolvand and M.R. Daymond, Internal strain and texture development during twinning: Comparing neutron diffraction measurements with crystal plasticity finite-element approaches, *Acta Mater.*, 60(2012), No. 5, p. 2240.
[111] H. Abdolvand and M.R. Daymond, Multi-scale modeling and experimental study of twin inception and propagation in hexagonal close-packed materials using a crystal plasticity finite element approach—Part I: Average behavior, *J. Mech. Phys. Solids*, 61(2013), No. 3, p. 783.
[112] H. Abdolvand and M.R. Daymond, Multi-scale modeling and experimental study of twin inception and propagation in hexagonal close-packed materials using a crystal plasticity finite element approach; part II: Local behavior, *J. Mech. Phys. Solids*, 61(2013), No. 3, p. 803.
[113] T. Hama, T. Suzuki, S. Hatakeyama, H. Fujimoto, and H. Takuda, Role of twinning on the stress and strain behaviors during reverse loading in rolled magnesium alloy sheets, *Mater. Sci. Eng. A*, 725(2018), p. 8.
[114] Q. Liu, A. Roy, and V.V. Silberschmidt, Temperature-dependent crystal-plasticity model for magnesium: A bottom-up approach, *Mech. Mater.*, 113(2017), p. 44.
[115] H.J. Zhang, A. Jérusalem, E. Salvati, C. Papadaki, K.S. Fong, X. Song, and A.M. Korsunsky, Multi-scale mechanisms of

twinning-detwinning in magnesium alloy AZ31B simulated by crystal plasticity modeling and validated via *in situ* synchrotron XRD and in situ SEM–EBSD, *Int. J. Plast.*, 119(2019), p. 43.

[116] J. Zhang and S.P. Joshi, Phenomenological crystal plasticity modeling and detailed micromechanical investigations of pure magnesium, *J. Mech. Phys. Solids*, 60(2012), No. 5, p. 945.

[117] J.D. Eshelby, The determination of the elastic field of an ellipsoidal inclusion, and related problems, *Proc. R. Soc. London*, *Ser. A*, *Math. Phys. Sci.*, 241(1957), No. 1226, p. 376.

[118] R. Hill, Continuum micro-mechanics of elastoplastic polycrystals, *J. Mech. Phys. Solids*, 13(1965), No. 2, p. 89.

[119] J.W. Hutchinson, Bounds and self-consistent estimates for creep of polycrystalline materials, *Proc. R. Soc. Lond. A*, 348(1976), No. 1652, p. 101.

[120] H. Wang, P.D. Wu, J. Wang, and C.N. Tomé, A crystal plasticity model for hexagonal close packed (HCP) crystals including twinning and de-twinning mechanisms, *Int. J. Plast.*, 49(2013), p. 36.

[121] H. Wang, P.D. Wu, and J. Wang, Modeling inelastic behavior of magnesium alloys during cyclic loading–unloading, *Int. J. Plast.*, 47(2013), p. 49.

[122] H. Qiao, S.R. Agnew, and P.D. Wu, Modeling twinning and detwinning behavior of Mg alloy ZK60A during monotonic and cyclic loading, *Int. J. Plast.*, 65(2015), p. 61.

[123] H. Qiao, X.Q. Guo, A.L. Oppedal, H. El Kadiri, P.D. Wu, and S.R. Agnew, Twin-induced hardening in extruded Mg alloy AM30, *Mater. Sci. Eng. A*, 687(2017), p. 17.

[124] G. Cailletaud and P. Pilvin, Utilisation de modèles polycristallins pour le calcul par éléments finis, *Rev. Européenne des Éléments Finis*, 3(1994), No. 4, p. 515.

[125] C. Yu, G.Z. Kang, and Q.H. Kan, Crystal plasticity based constitutive model for uniaxial ratchetting of polycrystalline magnesium alloy, *Comput. Mater. Sci.*, 84(2014), p. 63.

[126] C.O. Frederick and P.J. Armstrong, A mathematical representation of the multiaxial Bauschinger effect, *Mater. High Temp.*, 24(2007), No. 1, p. 1.

[127] H. Li, G.Z. Kang, and C. Yu, Modeling uniaxial ratchetting of magnesium alloys by a new crystal plasticity considering dislocation slipping, twinning and detwinning mechanisms, *Int. J. Mech. Sci.*, 179(2020), art. No. 105660.